HYDROGEN PRODUCTION FROM BIOMASS ON STRUCTURED CATALYSTS

A Thesis Submitted to
the Graduate School of Engineering and Sciences of
İzmir Institute of Technology
in Partial Fulfillment of the Requirements for the Degree of

DOCTOR OF PHILOSOPHY

in Chemical Engineering

by
Emin Selahattin UMDU

July 2012
İZMİR

We approve the thesis of **Emin Selahattin UMDU**

Examining Committee Members:

Assoc. Prof. Dr. Erol ŞEKER
Department of Chemical Engineering, İzmir Institute of Technology

Prof. Dr. Sacide Alsoy ALTINKAYA
Department of Chemical Engineering, İzmir Institute of Technology

Prof. Dr. Durmuş ÖZDEMİR
Department of Chemistry, İzmir Institute of Technology

Assoc. Prof. Dr. Oğuz BAYRAKTAR
Department of Chemical Engineering, İzmir Institute of Technology

Assoc. Prof. Dr. Ceylan ZAFER
Solar Energy Institute, Ege University

18 July 2012

Assoc. Prof. Dr. Erol ŞEKER
Supervisor, Department of Chemical Engineering, İzmir Institute of Technology

Prof. Dr. Mehmet POLAT
Head of the Department of
Chemical Engineering
Department

Prof. Dr. R. Tuğrul SENGER
Dean of the Graduate School of
Engineering and Sciences

ACKNOWLEDGEMENTS

It is pleasure to thank people who made this thesis possible. First, I would like to thank to my PhD supervisor Dr. Erol ŞEKER and thesis committee members Dr. Sacide ALSOY ALTINKAYA and Dr. Durmuş ÖZDEMİR for the encouragement, sound advices, good teaching and good ideas they provided. And I also want to thank Dr. ÖZDEMİR for his great help for liquid phase analysis. And for last but not least, I wish to thank my family and my friends for their support and understanding throughout the study.

ABSTRACT

HYDROGEN PRODUCTION FROM BIOMASS ON STRUCTURED CATALYSTS

The objective of this study is to investigate crystallite-size effect for oxides of transition metals iron supported on magnesium oxide (MgO) and cerium oxide (CeO_2) modified alumina (Al_2O_3) and the effect of the basicity and/or basic strength of support material, on activity and hydrogen selectivity in the steam reforming of glycerol.

Crystallite size effect is observed for MgO and Fe on MgO/Al_2O_3. It is observed that larger MgO crystallites size shifts gaseous product selectivity towards CO. Further as crystallite size is becomes higher than ~5 nm for Fe for gas product selectivity decreases. Basisity has also a similar behaviour; higher basisity or presence of unidentate carbonate basic sites observed at 865 and 800 cm^{-1} FTIR bands for CeO_2 promoted catalysts hinder CO formation and promotes CO_2 formation. This also results in high activity of steam reforming. Also basisity studies shows that inorganic carboxylate catalyst site with FTIR band 1535 and 1410 cm^{-1} is dominantly effective for gaseous product selectivity. High total basisity do not required for high glycerol conversion, yet high total basisity results in high gaseous product selectivity.

Considering studied catalysts and their catalytic activities it can be concluded that MgO and Fe modified catalysts shows better activity for syngas production due to their basic and crystalline properties. And CeO_2 modified catalysts or MgO catalysts with crystallite sizes lower than 5 nm are shows better performances for CO free product.

ÖZET

YAPISAL KATALİZÖRLER ÜZERİNDE BİYOKÜTLEDEN HİDROJEN ÜRETİMİ

Bu çalışmanın amacı seryum oksit (CeO_2) ve magnezyum oksit (MgO) ile modifiye edilmiş demir oksit geçiş metali destekli aluminanın (Al_2O_3) gliserol buhar dönüşümü için kristal boyutunun ve destek malzemesinin bazikliği ve bazik gücünün katalizörün aktivitesi ve hidrojen seçiciliği üzerine etkisini incelemektir.

MgO ve MgO/Al_2O_3 üzerinde Fe içeren katalizörlerde kristal büyüklüğü etkisi gözlenmiştir. MgO kristal büyüklüğü arttıkça gaz ürün seçimi carbon monoksite (CO) kaymaktadır. Ayrıca Fe kristal büyüklüğü ~5 nm üzerine büyüdükçe gaz ürün seçiciliği azalmaktadır. Baziklikde benzer bir davranış gösernektedir; daha yüksek baziklik yada CeO_2 yüklenmiş katalizörlerde 865 and 800 cm^{-1} FTIR bantlarında gözlenen monodentate carbonat CO oluşumunu engellemekte ve CO_2 üretimini arttırmaktadır. Bu aynı zamanda yüksek buhar riformu aktivitesine sebep olmaktadır. Ayrıca baziklik çalışmaları FTIR band 1535 and 1410 cm^{-1} ile belirlenmiş monodentate karboksilat bölgeleri gaz ürün seçiciliğinde baskın rol oynamaktaır. Yine de yüksek gliserol dönüşümü için yüksek toplam baziklik gerekmemektedir, ancak yüksek toplam baziklik gaz ürün dönüşümü için gereklidir.

Çalışılan katalizörler göz önüne alındığında MgO ve Fe içeren katalizörler bazik ve kristal özellikleri nedeniyle singaz üretimi için daha iyi aktivite göstermektedirler. Ve CeO_2 modifiye katalizörler yada Kristal boyutları 5nm'den küçük MgO katalizörler CO içermeyen ürünler için daha iyi performans göstermektedirler.

TABLE OF CONTENTS

APPENDICES

LIST OF FIGURES

Figure **Page**

LIST OF TABLES

Table **Page**

CHAPTER 1

INTRODUCTION

World energy consumption is increasing rapidly with both increasing population and increasing life standards all over the world and reached 474 exajoules in 2008. Transportation, which is mainly dependent on fossil fuels, is most rapidly growing sector with an average of 2.9 percent per year from 2004 to 2030 [International Energy Outlook 2007]. The expected sustainability of world proven reserves of oil is 42 years and proven reserves of natural gas is 60 years with current consumption trends [Balat 2009]. In addition to cost, there are significant environmental concerns with fossil fuel usage. Transportation is responsible for a significant amount of carbon dioxide and volatile organic compound (VOC) emissions, and a high contribution of carbon monoxide and nitrogen oxide (NO_x) emissions [Holladay 2009]. These emissions cause global warming, acid rains and direct effect on human health [Leung 2006]. Thus renewable alternative energy sources for a sustainable development are required to overcome these problems. Available sustainable energy sources are: solar, wind, hydro, biomass and geothermal energy. As, none of these can be directly used for transport purposes, thus these primary energy sources need to be converted to energy carriers such as electricity, hydrogen or bio-fuels.

Electricity which can be produced by numerous energy sources like heat, light or mechanical energy; has benefits in efficiency and availability for production, transmission, and consumption. Further it has zero emissions at end use. But efficient storage of large amounts of electrical energy is still a challenge. Considering large-scale production, bio-fuels may offer an opportunity for certain developing countries to reduce their dependence on oil imports. Unlike electricity biofuels do not require infrastructure changes and are compatible for conventional transport vehicles. They are also considered as zero emission fuels since carbon in the biofuels are reused by the plants. But their efficiencies are limited to those of engines which are about 20% of its energy converted into useful motivational power for internal combustion automobile engines. Comparing hydrogen with these other energy carriers, it has the highest specific energy content comparing conventional fuels. Hydrogen is the ideal fuel for its

high energy efficiency with fuel cell with efficiency up to 70% and generates only water as the waste product. Storage of hydrogen still requires further development, before being able to come close to the energy densities reached with fuels like gasoline and diesel.

Currently hydrogen is produced mostly from fossil fuels and water electrolysis [Marshall 2008]. Renewable hydrogen can be produced by electrolysis technology, biomass conversion to hydrogen by chemical routes, fermentation, of thermolysis, photolysis and via photo-biological ways [Turner 2008]. Basically the electrolysis of water is one of the simplest ways to produce hydrogen since it requires no moving parts, but a direct electric current (DC). Photo-electrochemical (PEC) splitting of water is another one-step process for hydrogen production where water is splitted directly with solar irradiation upon illumination. Biological ways for hydrogen production are also available. Dark fermentation, one of the biological pathways, which the metabolism of sugars, amino acids, and fatty acids results in the production of hydrogen, CO_2, and other products. The other one is photo-production by microorganisms which is similar in this way with photochemical splitting, the light is absorbed and the energy is used in charge separation reactions of photosynthesis. All these methods have some drawbacks as low efficiencies for biological systems or high operating and capital costs for electrolysis and photo-electrochemical systems. Biomass is one of the most abundant renewable resources varying from wood products from forestry, energy crops, agricultural residues, food wastes, or industrial wastes with a global generation of 150 GT of vegetable bio-matter every year and production of hydrogen from biomass has been proposed as a sustainable method to produce hydrogen. Variable feedstock compositions, need for efficient and durable catalysts for gas conditioning, and efficient heat integration are required for efficient conversion of biomass to hydrogen. There are three major thermochemical technology routes: gasification, pyrolysis/reforming, and high-pressure water/steam treatment [Turner 2008].

Among various biomass resources glycerol is a potential feedstock to produce H_2, because 1 mol of glycerol can theoretically produce up to 4 mol of hydrogen [Valliyappan 2008]. As a carbohydrate and sugar, glycerol has the same carbon/oxygen (C/O) ratio is internal C/O atomic ratio for glycerol is 1 as cellulose, about twice the oxygen content of pyrolysis oil [Shmid 2009]. Furthermore, glycerol is similar to pyrolysis oil in terms of density, viscosity, and energy content. Further glycerol markets

are limited and increase in biodiesel production in last decade results in large amounts of glycerol.

CHAPTER 2

LITERATURE REVIEW

Glycerol is a colourless, odourless, viscous liquid organic compound, also commonly called glycerine or glycerine. It is also backbone of triglycerides with a chemical formula $C_3H_5(OH)_3$. Its properties and structure are given in table 2.1. Over the last few years, the demand and production of biodiesel and also glycerol has increased tremendously as a by-product and glycerol synthesis becomes uneconomical. There is a downward trend in the glycerine market with a %70 decrease in crude glycerine, and % 60 decreases in kosher grade glycerol price between 1995 and 2005 [Singhabhandhu 2010]. Although its uses are versatile, there is a limited market for glycerol and several efforts are being made to utilize excess glycerol and produce value added products [Fernando 2009]. Recently glycerol draws a great attention for hydrogen production as a renewable source. Hydrogen production for renewable resource based technologies has lesser effects to the environment due to their carbon neutral nature. Hydrogen can be produced from glycerol via gasification and partial oxidation, autothermal reforming, aqueous-phase reforming (APR), supercritical water reforming processes and steam reforming. Studies about these processes in the literature are reviewed in this section.

Table 2.1. Properties and structure of glycerol

(Source: Mousdale 2008)

Molecular formula	$C_3H_5(OH)_3$	Glycerol structure
Density	1.261 g/cm³	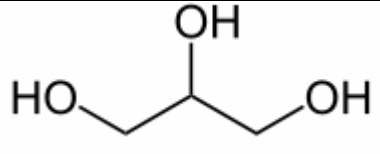
Melting point	18 °C	
Boiling point	290 °C	
Viscosity	1.5 Pa·s	

2.1. Hydrogen Production by Gasification and Partial Oxidation

In most basic terms gasification is a process related to pyrolysis performed in the presence of oxygen; in the form of air, pure oxygen or steam to chemically decompose condensed organic substances by heating. This process yields liquid fuels at low temperatures about 400 to 600 °C and gaseous products at high temperatures over 750 °C. In the partial oxidation process (PO_X), substrate is reacted with oxygen at sub-stoichiometric ratios, result in heat generation and high temperature. If excess oxygen is added, all the substrate is oxidized and produce mainly carbon dioxide and water [Adhikari 2009].

Schmid et al report that for catalytic partial oxidation process (CPOx) which occurs at high flow rates and millisecond contact times, transport effect shall also be considered. Previous studies showed that higher conversion to equilibrium products occurs at a greater pore density (smaller pores) of catalyst, whereas non-equilibrium products are favored by larger pores. Another factor effecting the product distribution is catalyst itself. Rhodium-based catalysts tend to produce equilibrium products which are C1 gases, H_2, and water with high conversion. Pt catalysts can be used to select non-equilibrium products, as hydroxypropionaldehyde or hydroxyacetone especially those produced by thermal decomposition or dehydrogenation. Although their aim was to produce syngas from glycerol. Their results showed that H_2 selectivity has a maximum under their reaction conditions over the Rh/Ce catalyst in about 1.2 C/O molar ratio [Schmid 2009].

2.2. Hydrogen Production by Autothermal Reforming

ATR (autothermal reforming) is a combination of steam reforming (SR) and partial oxidation process (PO_X). Comparing pyrolysis and SR, which will be mentioned in detail later, ATR does not require an additional/external heat supply. ATR get thermal energy required by production of some complete oxidation products in the highly exothermic combustion reaction and uses this energy in a reaction which oxygen, steam, and fuel are all reactants [Alikari 2009]. Thermodynamic analysis of ATR for

glycerol shows that high temperatures, high steam/glycerol ratios and low oxygen/glycerol ratios are preferable for this process [Ma 2009].

Study of Shmid et al shows that higher steam/carbon ratio results in higher H_2 selectivity at low C/O ratios, lower CO selectivity and higher acetaldehyde formation over Pt and Rh on Al_2O_3 between 700 to 1200 °C. Further; addition of Ce to Rh raised the synthesis gas selectivity by ~10% due to ability of Ce to store oxygen making it available for surface reactions on Rh. In the case of Pt, less H_2 has produced than Rh at higher C/O ratios because of the C–O bond scission which could result in increased the level of adsorbed carbon [Schmid 2006].

2.3. Hydrogen Production by Aqueous-Phase Reforming

Cortright et al. introduced a new method, that hydrogen could be efficiently produced from model biomass glucose and biomass-derived polyols at mild conditions around 500 °K in a single-reactor by aqueous-phase reforming (APR) process [Cortright 2002]. Compared to other processes, vaporization of water and oxygenated hydrocarbons are not needed in this process, and process is energy saving considering the others. Further higher low operating temperatures increases water–gas shift (WGS) reaction, which is thermodynamically favoured. This leads to low levels of CO and high hydrogen selectivity about 70%, but they also reported that conversion of glycerol also decreased to 10% w/w on 3% Pt/Al_2O_3. Moreover they observed undesired homogeneous reactions even with H_2O/C molar ratio of 165, and they increase the reaction with decreasing molar ratio especially for glucose. Theoretically APR of glycerol occurs according to the following the overall reaction;

$$C_3H_8O_3 + 3H_2O \rightarrow 7H_2 + 3CO_2 \quad (2.1)$$

This includes two other main reactions in it:

$$C_3H_8O_3 \rightarrow 4H_2 + 3CO \quad (2.2)$$

$$CO + H_2O \rightarrow H_2 + CO_2 \quad (2.3)$$

Second reaction above is C–C cleavage and third one is water–gas shift. These two reactions are related to the nature of the metal, yet basicity and acidity of the support also was also reported to be effective on the activity and gas distribution remarkably [Wan 2008]. It has also stated that a good catalyst for production of H_2 by aqueous-phase reforming should facilitate C-C bond cleavage and promote removal of adsorbed CO species by the water-gas shift reaction, but the catalyst must not facilitate C-O bond cleavage and hydrogenation of CO or CO_2. Wan et al studied the effect of metal and support (acidity and basicity) on the activity and stability of APR reaction. Their study showed that Pt had high activity and high hydrogen concentrations achieved since it has high activity for C–C bond breaking and WGS, and low activity for methanation. It was also reported that Cu had significant high activity for the WGS reaction, whereas remarkably low activities for the C–C cleavage reaction. They also observed that methanation reaction was observed over Cu catalysts. Yet both Ni and Co shows both low activity and stability because of the severe loss of exposed metal active sites, which would be attributed to the crystallization of the support, the sintering of the metal particles, oxidation of the metal sites, and the carbon deposition during the APR reaction conditions. Further their results showed that the effect of metal particle size was not dominant on the four catalysts; Pt/Al_2O_3, Pt/SiO_2, Pt/AC, and Pt/HUSY. Furthermore they reported that zeolite structures collapsed under the reaction conditions. Strangely they observed highest activity for Pt on Al_2O_3 which could be considered neutral considering other supports. The reason for this behaviour was that the severe adsorption of CO_2 on MgO causes formation of $MgCO_3$ phases and loss of MgO content on support.

Another catalyst property, metal particle size was also studied for hydrogen selectivity of the APR reaction using glycerol. Different platinum salts were used to control the Pt particle size with a 3% w/w load on Al_2O_3 [Lehnert 2008]. Lehnert et. al. reported that APR reaction was structure sensitive for selectivity which increases with particle size, but the rate of reaction is not affected. They propose that an increase in the particle size resulted in an increase of the number of terrace atoms of the metal crystallite and decrease in number of edge and corner atoms declines. Hence, they suggested that the adsorption of the oxygenated hydrocarbon for subsequent cleavage of a C–C bond could be realized preferably at face positions. In the same study this trend also observed with increased particle size by increased metal load from 1% to 10.

In addition, metal and support the addition of promoters as in the case of Sn to Ni catalysts showed decreased the rates of alkane hydrogenolysis reactions and enhanced the selectivity to dehydrogenated products [Shabaker 2004]. It was reported that the primary effect of adding Sn to Ni must be the suppression of the C–O bond cleavage and methanation reactions, while maintaining sufficient catalytic activity for the cleavage of C–C bonds.

2.4. Hydrogen Production by Steam Reforming

In the steam reforming, substrate is reacted with steam in the presence of a catalyst to produce hydrogen, carbon dioxide, and carbon monoxide. It is the most commonly used method for hydrogen production in chemical industry [Alikari 2009]. This process is composed of mainly two reactions. First reforming reaction, which is mainly involve splitting of hydrocarbons in the presence of water known as steam reforming, and second one is water–gas shift (WGS) reaction. These reactions can be summarized as;

$$C_3H_8O_3 \xrightarrow{H_2O} 3CO + 4H_2 \quad (2.4)$$

$$CO + H_2O \rightarrow CO_2 + H_2 \quad (2.5)$$

Although the WGS is exothermic, reforming reactions are highly endothermic taking more heat evolved from WGS reaction, therefore, overall reaction is an endothermic process and increased glycerol conversion is observed with increased temperature [Adhikari 2008]. The overall reaction of steam reforming can be given as;

$$C_3H_8O_3 + 3\ H_2O \rightarrow 7\ H_2 + 3\ CO_2 \quad (2.6)$$

In fact the real reaction mechanism is more complicated as seen in figure 2. And there are still other products to minimize, and CO is needed to be converted for applications in fuel cells. Low temperatures and high WGS are desired to minimize CO formation; however less hydrogen is produced under the conditions that favour the inhibition of CO [Ma 2008]. In case of CO_2, its formation increases with increasing

temperature up to about 850 °K, and then decreases at higher temperatures possibly due to methanation reaction can be summarized as;

$$CO + 3\ H_2 \rightarrow CH_4 + H_2O \qquad (2.7)$$

This also affects H_2 selectivity negatively. Further it is also reported that best conditions to produce hydrogen will be with excess water and at low pressures [Fernando 2007, Ma 2008]. Another reaction parameter affecting the H_2 selectivity is temperature increased selectivity is observed for increased temperature [Adhikari, 2008]. Buffoni et. al. reports that 550 °C is the minimum temperature required to obtain hydrogen with high selectivity [Buffoni 2009]. It was also reported that first dehydrogenation step on the metal surface to give adsorbed intermediates for the cleavage of C–C or C–O bonds of glycerol molecule is necessary. In nickel catalysts, the strong capacity for breaking the C–C bond would lead to formation of CO and H_2. Also a higher contribution of temperature increase in the steam reforming reaction rather than the glycerol decomposition reactions reported. Similarly at higher temperatures contribution to methanation reaction is lower. At temperatures lower than 450 °C the capacity to break C–C bonds is lower and formation of liquid phase unsaturated compounds increased [Buffoni 2009, Ding 2009]. Generalized reaction paths are shown in Figure 2.1.

Buffoni et al reports that their experimental results are in agreement with the literature that it is necessary a first dehydrogenation step on the metal surface to give adsorbed intermediates for the cleavage of C–C or C–O bonds of glycerol molecule. In nickel catalysts, the strong capacity for breaking the C–C bond would lead to formation of CO and H_2. Further they also state that temperature increase results higher contribution of the steam reforming reaction than the glycerol decomposition reaction. Similarly at higher temperatures contribution is lower to methanation reaction which results in lower methane formation. At temperatures lower than 450 °C the capacity to break C–C bonds is lower, thus dehydrogenated intermediates reacts in dehydration and rearrangement in presence of support acid sites reactions and forms liquid phase unsaturated compounds [Buffoni 2009, Ding 2009].

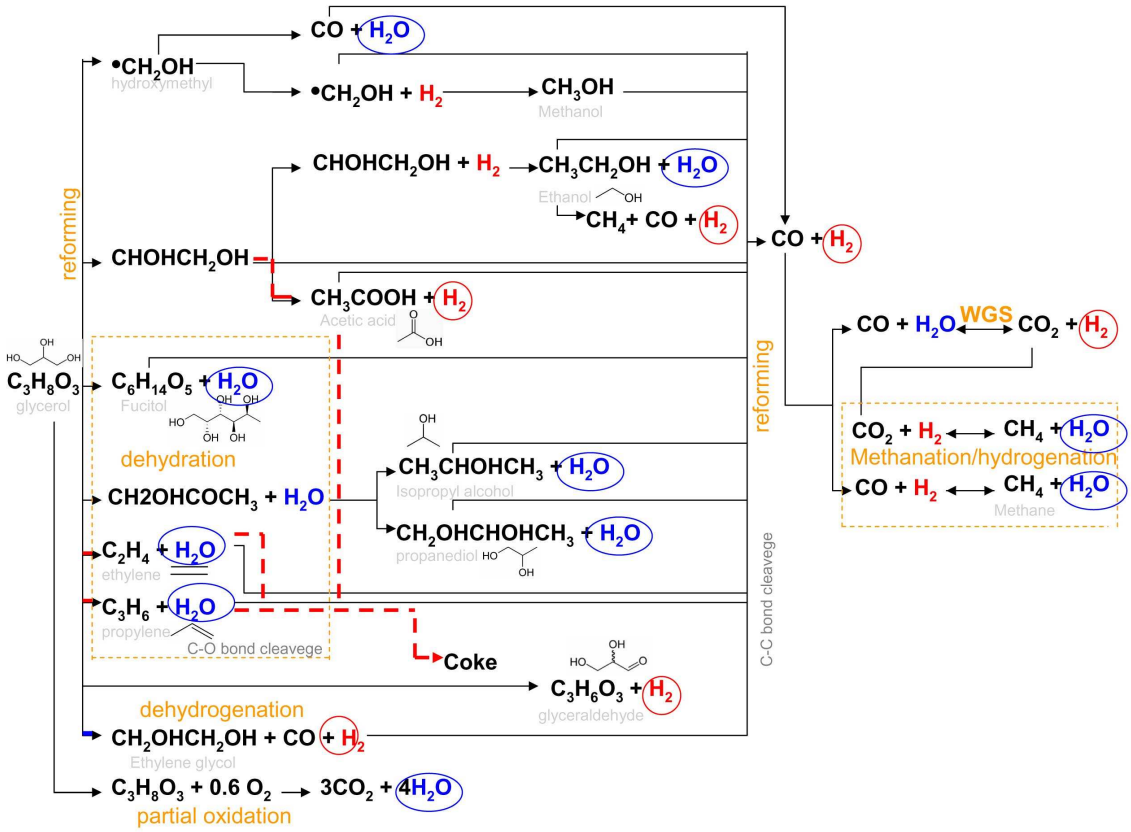

Figure 2.1. Some of the possible reactions that may occur in hydrogen production from glycerol by steam reforming (Source: Adhikari 2009, Somoraj 1994, Xiao 2008).

Suziki et. al. reported that activity order of group 8-10 metals for steam reforming are in order as Ru ~ Rh > Ni > Ir > Co > Pt > Pd > Fe on Y_2O_3 at 600 °C [Suziki 2005]. Yet Fernando et. al. reports that H_2 selectivity for the reaction at 900 °C was in the order: Ni > Ir > Ru > Pt > Rh, Pd and glycerin conversion for the reaction at 900 °C was in the order: Ni > Ir > Pd > Rh > Pt > Ru [Fernando 2007]. Although temperatures are highly different this also shows an important contribution of support to the reaction. But in these studies crystallite sizes do not considered. As stated before Lehnert et al shows that APR reaction is structure sensitive and crystallite size is an important factor for selectivity [Lehnert 2008]. Buffoni et al shows support effect on activities of supported Ni catalyst at relatively similar Ni crystallite size of 14 to 18 nm, but they do not study effect of crystallite sizes. Ni is considered as highly active compared to others such as Ru, Rh, Ir, Co, Pt, Pd or Fe. High coke formation on Ni catalysts which result in decreased catalyst activity with time is also reported [Suziki

2005, Fernando 2007]. Coke formation is also reported as a possible cause for formation of carbonaceous products other than catalyst deactivation and indirectly as a cause [Cominelli 2010]. A study to evaluate the effect of the support in steam reforming of glycerol shows that the acidity of supports promotes dehydration, dehydrogenation, hydrogenolysis and condensation reactions resultant in coke formation causing fast deactivation of catalysts [Pompeo 2010]. Yet acidity of the catalysts is inspected only indirectly and qualitatively. But another study reported that at least two types of carbonaceous deposits forms on over bimetallic Co-Ni/Al_2O_3 where one of these carbon deposits was resistant to removal with H_2 regeneration cycles [Adesina 2010]. The high selectivity towards hydrogen and catalytic stability can be achived by B_2O_3. The Ni-B amorphous alloy catalyst also was found to be more active in terms of the H_2 production rate and more selective toward H_2 as compared to skeletal Ni [Guanzhong 2012].

Adhicari et al. also had given crystallite sizes for basic supports and reported decreasing H_2 selectivity and glycerol conversion for CeO_2, MgO and TiO_2. They contribute this change to the CH_4 reforming but did not give any clues about any relationship with catalysts properties [Adhikari 2008]. Studies on APR reaction are shows that these reactions are structure sensitive and crystallite size is an important factor for selectivity [Lehnert 2008] and similarly this can be also a contributing factor in catalyst performance. CeO_2 may act as water gas shift catalysts by reduce H_2O and oxidize CO in the production of H_2 and CO_2. Through this process each reaction of a CO molecule with the ceria to form CO_2 removes one oxygen atom from the ceria lattice and two electrons remain at the vacancy result a new site [Swanson 2008].

Low interactions between meat and support resulting in Ni oxidation and thus deactivation for Ni/TiO_2 catalysts reported. Low activity in C-C bond cleavage especially at low temperatures is lower and secondary reactions (dehydration, rearrangement and condensation) are favoured, leading to the formation of unsaturated compounds which are good precursors in coke deposition [Nichele 2012]. But this effect is mostly observed at high conversions. Selectivity to primary products reported to decrease, while the selectivity to gas increase at high conversions; while primary products dominate the carbon selectivity, with smaller amounts of gas and secondary products at low conversions [Dietrich 2012]. A recent study on NiO supported catalysts shows that $NiTiO_3$ formed at high temperatures by interdiffuse of NiO and TiO_2 is still reducible to NiO and stays active in the partial oxidation of methane. Further it is reported that high activity in glycerol steam reforming, with total glycerol conversion

and selectivity to hydrogen of about 90%. But this reduction requires higher temperatures than NiO [Nichele 2012].

Independently from the catalyst (Rh or Ni) used in the study of Chiodo et al and temperature investigated glycerol is subjected to pyrolysis and drastically decomposes before it to reach the catalyst surface at temperatures higher than 720 K. Rh/Al_2O_3 catalyst reported be more active and stable than Ni supported catalysts and either of the catalysts affected by coke formation mainly promoted by the large presence of olefins formed by glycerol thermal decomposition. At high temperatures glycerol easily decomposes into CO, CO_2, olefins, water hydrogen and oxygenates before to reach the catalytic surface. Results of reaction at 1073K indicated that glycerol significantly decomposes (conversion close to 65 mol%) for using a reaction stream containing 7% of glycerol. Composition of the product stream was reported as CO (upper 50 mol%), CO_2 (1 mol%), olefins (ethylene and propylene about 25 mol%), CH_4 (~13 mol%) and H_2 (~10 mol%). These results in coke formation due to the large presence of olefins in the reaction stream, formed by glycerol thermal decomposition independently from the catalyst used (Rh or Ni) and temperature investigated [Chiodo 2010]. Similar observations also reported by Chen et. al. [Chen 2010] and Pompeo et al [Pompeo 2011]. Lower total conversion of Ni than Pt catalyst in the same experimental conditions reported similar to Rh [Pompeo 2011]. In fact an alternative for single-stage production of hydrogen, a sorption enhanced steam reforming provides CO_2 removal from the system is proposed in this study. They achieve high hydrogen content and by very low levels of CO, CO_2 and methane levels in the downstream due to the equilibrium shift effect of in situ CO_2 removal. Yet reduction in hydrogen yield and promotion of carbon formation observed and it is reported that pyrolysis of glycerol before or when it passed through the catalytic bed is believed to be responsible for this observations. Other than these observations increasing coking reaction with respect to the gasification reaction resulting in pore blocking and deactivating the catalyst for powder and the pellet catalysts [Bobadilla 2012].

Table 2.1. Selected catalysts performances from selected studies for H_2 production from glycerol.

Catalyst	Catalyst load (w/w%)	T (°C)	Glycerol Feed	H_2 Selectivity (%)	Glycerol Conversion (%)	Reference
Ni/CeO_2	11.6/88.4			66	100	
Ni/MgO	9.6/91.4	650	6:1 WGMR	52	100	Adhikari, 2008
Ni/TiO_2	12.7/87.3			47	83	
Pt/C	5/95	350	30% w/w	-	61	Soares, 2006
Ni/MgO				66	100	
Ni/CeO_2	15/85	650	60% w/w	54	93	Adhikari 2008
Ni/TiO_2				62	98	
$Ni/La_2O_3/Al_2O_3$	6/6/88			100		
$Pt/La_2O_3/Al_2O_3$	6/6/88	500	9:1 WGMR	27	100	Güemez 2009
$Ni\text{-}Pt/La_2O_3/Al_2O_3$	6-6/6/82			87		
Ni/Al_2O_3	2/98			40	50	
$Ni/CeO_2/Al_2O_3$	2/5/93	600	9:1 WGMR	75	96	Buffoni 2009
$Ni/ZrO/Al_2O_3$	2/5/93			99	80	
Ru/Y_2O_3	3/97	600	3.3:1	88	100	Suzuki 2005
$Ru/CeO_2/Al_2O_3$	2.5	900	6:1 WGMR	71	94	Adhikari 2007
$Ni/CeO_2/Al_2O_3$				80	94	
Ni/TiO_2	10	650	10% w/w	5	10	Nichele 2012
Ni/SiO_2	2	450	10% w/w	68	42	Pompeo 2011
$NiSn/MgO/Al_2O_3$	26/15	750	4	30	-	Bobadilla 2012

An other important factor for coke formation is the decomposition of glycerol before it to reach the catalyst surface at temperatures higher than 720 K independent from the catalyst (Rh or Ni) used in the study of Chiodo et al Rh/Al_2O_3 catalyst reported be more active and stable than Ni supported catalysts and either of the catalysts affected by coke formation mainly promoted by the large presence of olefins formed by glycerol thermal decomposition. At high temperatures glycerol easily decomposes into CO, CO_2, olefins, water hydrogen and oxygenates before to reach the catalytic surface. Results of reaction at 1073 ºK indicated that glycerol significantly decomposes (conversion close

to 65 mol%) for using a reaction stream containing 7% of glycerol. These results in coke formation due to the large presence of olefins in the reaction stream, formed by glycerol thermal decomposition independently from the catalyst used (Rh or Ni) and temperature investigated [Chiodo 2010]. Similar observations also reported by Chen et al [Chen 2010]. In fact an alternative for single-stage production of hydrogen, a sorption enhanced steam reforming provides CO_2 removal from the system is proposed in this study. They achieve high hydrogen content and by very low levels of CO, CO_2 and methane levels in the downstream due to the equilibrium shift effect of in situ CO_2 removal. Yet reduction in hydrogen yield and promotion of carbon formation observed and it is reported that pyrolysis of glycerol before or when it passed through the catalytic bed is believed to be responsible for this observations.

Contribution of support to the reaction is known important for these reactions [Tanabe, 1989]. Support acid sites would lead to the appearance of products identified in liquid phase dehydration reactions. Decreasing H_2 selectivity and glycerol conversion were reported for CeO_2, MgO and TiO_2 supported catalysts respectively. Basic character of Ce support decreases unsaturated compounds [Buffoni 2009]. Similarly supports can be modified with alkaline-earth oxides such as to reduce the acidity of the support, to prevent metal sintering and to avoid catalyst deactivation as in the study of Güemez et al to modify alumina with La_2O_3. This modification results in only gas products by reducing acidic nature of the Al_2O_3 and improves reactions for the oxygenated hydrocarbons (OHCs) conversion into CH_4, CO, CO_2 and H_2. Further increasing the La/Al ratio the hydrogen production increases, reaching a maximum for a 6% of lanthana, and decreases for higher La/Al ratios [Güemez 2009]. Yet Soares et al also shows that Al_2O_3, ZrO_2, CeO_2/ZrO_2, and MgO/ZrO_2 supported Pt catalysts exhibited deactivation during time-on-stream, where the Pt/C catalyst showed stable conversion [Soares 2006]. Adhikari et al reports a similar deactivation for CeO_2. H_2 selectivity of CeO_2 supported catalyst decreased with increased temperature where it increases for TiO_2, and at the same conditions MgO shows relatively no change [Adhikari 2008]. They report that strong adsorption of CO_2 on basic sites results on deactivation for these catalysts. Although effects of basic promoters are studied there is little information about the basicity and basic strength of the active sites in these studies.

Supports can be modified with similar alkaline-earth oxides to reduce the acidity of the support, to prevent metal sintering and to avoid catalyst deactivation. La_2O_3 modified alumina results in only gas products by reducing acidic nature of the Al_2O_3

and improves reactions for the oxygenated hydrocarbons (OHCs) conversion into CH_4, CO, CO_2 and H_2 [Güemez 2009].

Further study of Sutar et el shows that a first order kinetic is observed for glycerol over Pt/C catalysts. Further they report that practically there is no change observed in the glycerol conversion at 773 ºK by changing the total volumetric flow rate in the range of 160 to 310 cm^3/ min at a space time equal to 1.56 g h/mol. A similar result was observed when they change particles in the size range of 150 to 210 μl. Thus they claim that the external mass transfer resistance and pore diffusion limitation was absent over the entire temperature range studied for their system [Sutar 2010]. Reactor space time effects gaseous product distribution. Increase in CO_2 and H_2 production at the expense of CO decrease is reported with the increased space time [Pompeo 2011].

CHAPTER 3

EXPERIMENTAL

3.1. Materials

Currently two mixed oxide catalyst groups were synthesized; Fe on CeO_2/Al_2O_3 and Fe on MgO/Al_2O_3. In the synthesis of the catalysts, magnesium nitrate hexahydrate (Alfa Easer) was used as a precursor for magnesium oxide and Cerium(III) nitrate hexahydrate (Alfa Easer) as precursor for cerium oxide. Aluminum isopropoxide (AIP) were used as precursors for alumina support oxides. Deionised water (DIW) were used as solvent and nitric acid (HNO_3) were used as peptizer in the sol-gel method. Used chemicals are summarized in the Table 3.1.

Table 3.1. Properties of materials used in mixed oxide support synthesis.

	Chemical formula	Molecular Weight (g/mol)
Aluminum isopropoxide	$Al(OCH(CH_3)_2)_3$	204.24
Magnesium nitrate hexahydrate	$Mg(NO_3)_2 \cdot 6H_2O$	256.41
Cerium(III) nitrate hexahydrate	$Ce(NO_3)_3 \cdot 6H_2O$	434.22
Iron(III) nitrate	$Fe(NO_3)_3 \cdot 9H_2O$	403.999

3.2. Catalysts Preparation

4 different mixed designs used for the selection of catalysts loadings. These designs are Fe on CeO_2/Al_2O_3, Fe on MgO/Al_2O_3, Pt on CeO_2/Al_2O_3 and Pt on MgO/Al_2O_3. Two of these designs that are containing iron are synthesized. A list of catalysts that were prepared is given in Table 4.1 and Table 4.2. Each design has 3 factors; transition metal load %w/w and basic promoter load %w/w and support amount wt. %. 2 different basic promoters and 2 different metals are considered in each of these designs. Simplex design is applied with upper limits of 10% for Fe and 50% for MgO and CeO_2 involving components of a mixture, where the levels of the components are constrained to sum to 100%.

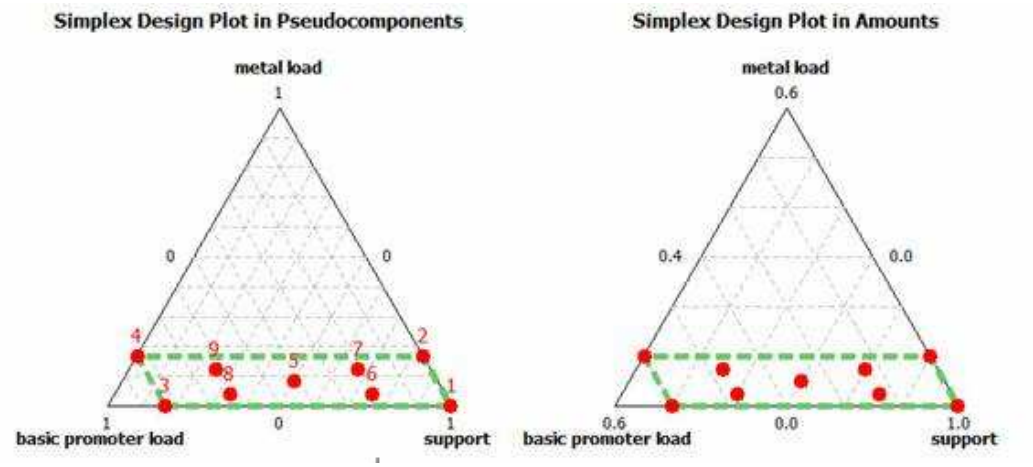

Figure 3.1. Design plots of synthesized catalysts.

Table 3.2. Fe on MgO/Al_2O_3 Catalyst prepared and their weight percentages.

Catalyst code	**StdOrder**	**PtType**	**Blocks**	**wt. % Fe on MgO/Al_2O_3**	**wt. % MgO**	**wt. % Al_2O_3**
MF1	1	1	1	0	0	100
MF2	2	1	1	10	0	90
MF3	3	1	1	0	50	50
MF4	4	1	1	10	50	40
MF5	5	0	1	5	25	70
MF6	6	-1	1	2.5	12.5	85
MF7	7	-1	1	7.5	12.5	80
MF8	8	-1	1	2.5	37.5	60
MF9	9	-1	1	7.5	37.5	55

Table 4.3. Fe on CeO_2/Al_2O_3 Catalyst prepared and their weight percentages.

Catalyst code	**StdOrder**	**PtType**	**Blocks**	**wt. % Fe on CeO_2/Al_2O_3**	**wt. % CeO_2**	**wt. % Al_2O_3**
CF1	1	1	1	0	0	100
CF2	2	1	1	10	0	90
CF3	3	1	1	0	50	50
CF4	4	1	1	10	50	40
CF5	5	0	1	5	25	70
CF6	6	-1	1	2.5	12.5	85
CF7	7	-1	1	7.5	12.5	80
CF8	8	-1	1	2.5	37.5	60
CF9	9	-1	1	7.5	37.5	55

Mixed oxide catalyst supports were synthesized by a modified single step sol-gel method. In the synthesis of the supports, magnesium nitrate hexahydrate will be used as a precursor for magnesium oxide, Cerium(III) nitrate hexahydrate as precursor for cerium oxide respectively. Aluminum isopropoxide (AIP) precursors for alumina support. Deionised water (DIW) used as solvent and nitric acid (HNO_3) used as peptizer in the sol-gel method. Purities of chemicals that used are summarized in the Table 4.2. Preparation of catalyst starts mixing necessary amounts of alumina isopropoxide (AIP) and water at 85 ºC under total reflux for 1 h. Then HNO_3 is added to the mixture and stirred at the same temperature for another hour. After that needed amounts of magnesium and cerium precursors added and stirred for 30 min at the same temperature. Then metal precursors added and stirred at the same temperature and for 30 minutes. Finally, excess water removed with slow evaporation to obtain the mixed oxide gel. All the gels will be dried at 120 ºC for 18 h. The catalysts were calcined at 600 °C for 6 h. The catalysts grounded and sieved for less than 80 mesh and stored in the desiccators.

3.3. Solid Oxide Catalyst Testing in Glycerol Reforming

Figure 4 shows a schematic diagram of the reaction system used for the catalytic steam reforming of glycerol. A continuous flow fixed-bed reactor placed in an oven

with temperature control. The reforming reaction took place in a quartz pipe with 6mm diameter. The reactor was placed inside a furnace to provide temperature control. Catalysts will be tested for activity and product selectivity for 400, 450 and 500 °C. A helium flow served as a carrier.

Glycerol contains higher oxygen content and has an oxygen/carbon ratio of 1 thus it is already at the carbon boundary and does not need any extra oxygen or hydrogen to prevent carbon deposition of solid carbon particles exist in equilibrium with the gaseous components [Slinn 2008]. Yet as stated before H_2 selectivity is increasing with excess water present in the reaction [Adhikari 2007, Ma 2008]. Higher WGR values do not contribute H_2 selectivity significantly when higher than 9:1 WGR at approximately 600 °C by closing to the stoichiometric value [Ma 2008]. Thus water/glycerol ratios (WGR) of 3:1 chosen for reaction conditions. As stated before hydrogen can be produced from dehydrogenation of glycerol at lower temperatures to yield carbonyl products such as acetol, di-hydroxy acetone and glyceraldehyde without C-C cleavage and this decreases H_2/CO ratio [Kunkes 2009].

Glycerol and water mixture pumped into the evaporator and heated to 310 °C to vaporize subsequently mixed with the diluting carrier stream. The glycerol in the feed gas composition will be kept 1 vol% to prevent saturation in the gas stream. All flow lines carrying glycerol will be kept at 300 °C to prevent condensation. The space velocity is kept as weight hourly space velocity (WHSV) 9.6 h^{-1} and gas hourly space velocity (GHSV) 22500 h^{-1} for 0.1 g of catalyst fed into 6mm outer diameter quartz reactor. The high space velocity required to obtain partial conversion means that there will be no back diffusion of hydrogen [Ertl 2008].

Hydrogen and CO_2, CO, methane content in the reactor outlet gas stream analyzed with TCD. Liquid phases are collected and stored in air tight container in refrigeration. GC analysis by using a Shimadzu GC-17A gas chromatograph equipped with a Shin Carbon ST 80/100 column and TCD detector. Column temperature kept at 40 ºC for 3 min then heated up to 250 ºC with 8 ºC/min increment then stayed at that temperature for 10 min. Other parameters are given as below:

Column pressure	: 130
Injection Port Temperature (ºC)	: 100
Detector Temperature (ºC)	: 200
Detector Current (mA)	: 50
Detector range	: 1

The separation was achieved using a non-isothermal analysis method: Column temperature kept at 40 ºC for 3 min then heated up to 250 ºC with 8 ºC/min increment then stayed at that temperature for 10 min. The injection port is maintained at 100 C˚ and detector maintained 200 ºC. Detector Current was 50 mA and detector range was 1. Carrier gas helium pressure was set to 130 kPa. The sample injection size was 5 mL. GC analysis of liquid phase blank tests shows that with increased temperature product distribution and their intensities changes.

FTIR spectroscopic measurements of the samples were carried out in diffuse reflectance mode and raw spectra used for calibration sets and independent validation sets. Multivariate calibration models were built with genetic inverse least squares (GILS) method applied for determining concentrations [Özdemir 2011].

Liquid phases of selected catalysts are also inspected qualitatively for determination of liquid phase products. A Perkin Elmer Clarus 600 gas chromotograph with a FID detector and a SGE G7 BP20 column. Column temperature kept at 40 ºC for 3 min then heated up to 200 ºC with 10 ºC/min increment then stayed at that temperature for 15 min. Injection port kept at 200 ºC and injection volume was 2 μL and column flow kept 1 ml.

3.4. Catalyst Characterization

In the characterization of the samples, X-ray diffraction (XRD), BET and TPD were used. XRD pattern of the samples were determined using a Philips Xpert XRA-480 Model X-ray diffractometer. XRD patterns were analyzed to find out the crystallite phase and also the average crystallite sizes using the Scherrer equation given below:

$$T = K \lambda / (B \cos\theta) \qquad (3.1)$$

Where T is crystal thickness, K is Scherrer constant (~0.9-1), λ is wavelength of the X=ray, B is the broadening of a diffracted peak found using the full width at half maximum in terms of radian and θ is diffraction angle in degrees (Patterson 1939).

BET analysis was used to calculate the porosity and the specific surface area of the oxide samples. The measurements were performed by Micrometrix Gemini V at scan mode at 77.35 ºK in the presence of N_2.

Fourrier Transfer Infra Red (FTIR) is used to determine number and base or acid strength of sites on a solid surface with an adsorbed gas. Carbon dioxide (CO_2) is used as adsorbed gas to determine strength of basic sites, and HNO3 used for observation of acidic sites. First catalysts are activated by heating up to 600 ºC with 10 ºC/min heating rate and kept at that temperature for 1 h and cooled to room temperature under helium flow. Then adsorption is carried out for 1 h at room temperature with a total of 70 mL/min probe gas flow over 100 mg catalyst. After that catalysts were cooled to room temperature. Both activated and cooled catalysts and probe molecule adsorbed catalysts grinded with KBr and then compressed to form pallets. These pallets are observed by Shimadzu-8400S Fourier Transform Infrared Spektrometry for 400 – 4000 1/cm. Probe adsorbed catalysts are compared with only activated catalysts and emerged peaks are inspected. Quantification of observation is carried over by adsorption of CO_2 by dosing known amounts of probe gas into air tight vessels under nitrogen atmosphere. Change in CO_2 concentration monitored by gas chromatography. The results also compared with FTIR results of used catalysts and fresh catalysts.

CHAPTER 4

RESULTS AND DISCUSSION

4.1. Catalyst Characterization

XRD patterns of the samples were determined using a Philips Xpert XRA- 480 Model X-ray diffractometer. XRD patterns were analyzed to find out the crystalline phases and crystallite sizes. The average crystallite sizes were calculated using the Scherrer equation given below:

$$T = K \lambda / (B \cos\theta) \quad (4.1)$$

where T is crystal thickness, K is Scherrer constant (~0.9-1), λ is wavelength of the Xray, B is the broadening of a diffracted peak found using the full width at half maximum in terms of radian and θ is diffraction angle in degrees (Patterson 1939).

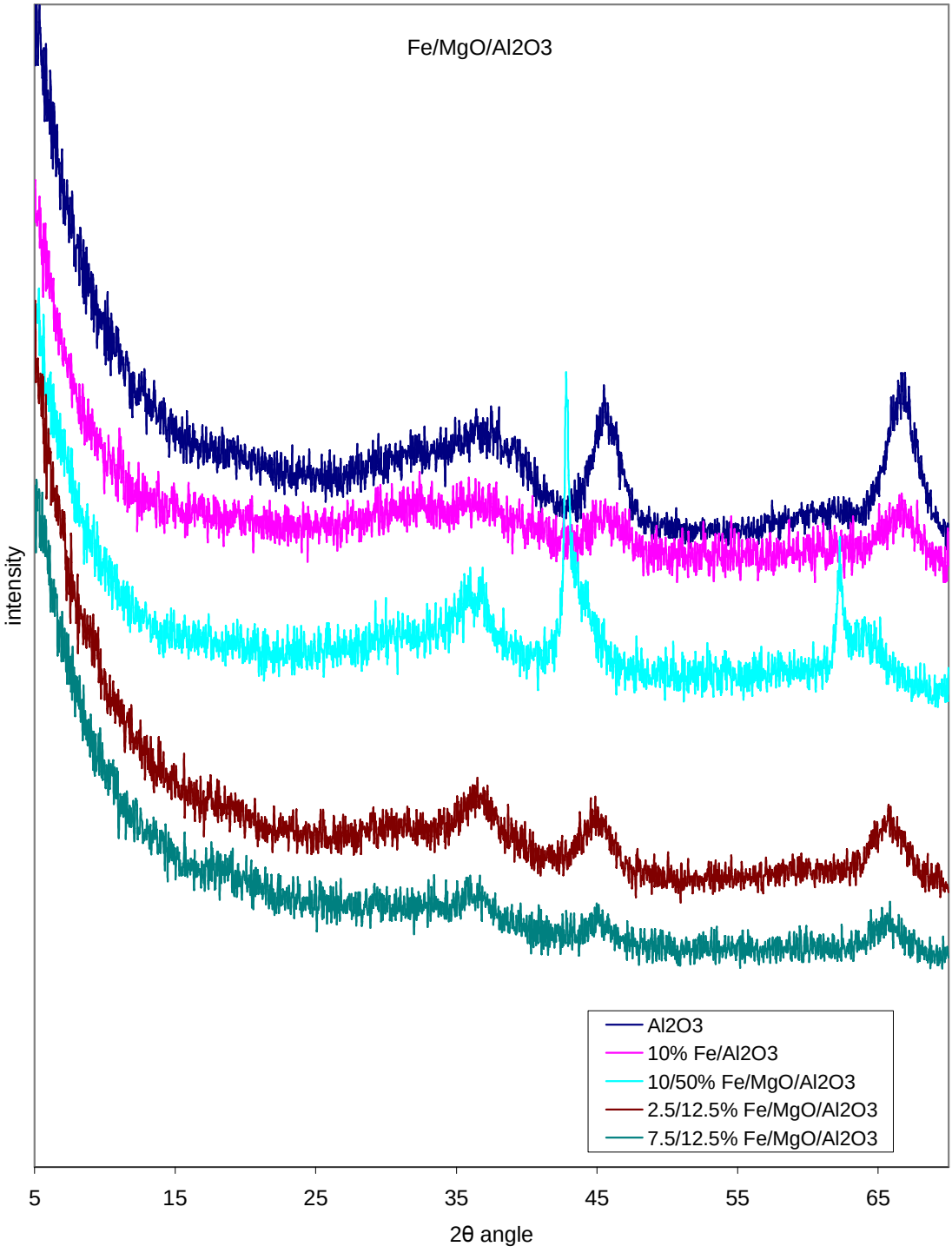

Figure 4.1. Comparison of XRD patterns for Fe on MgO/Al_2O_3 catalysts.

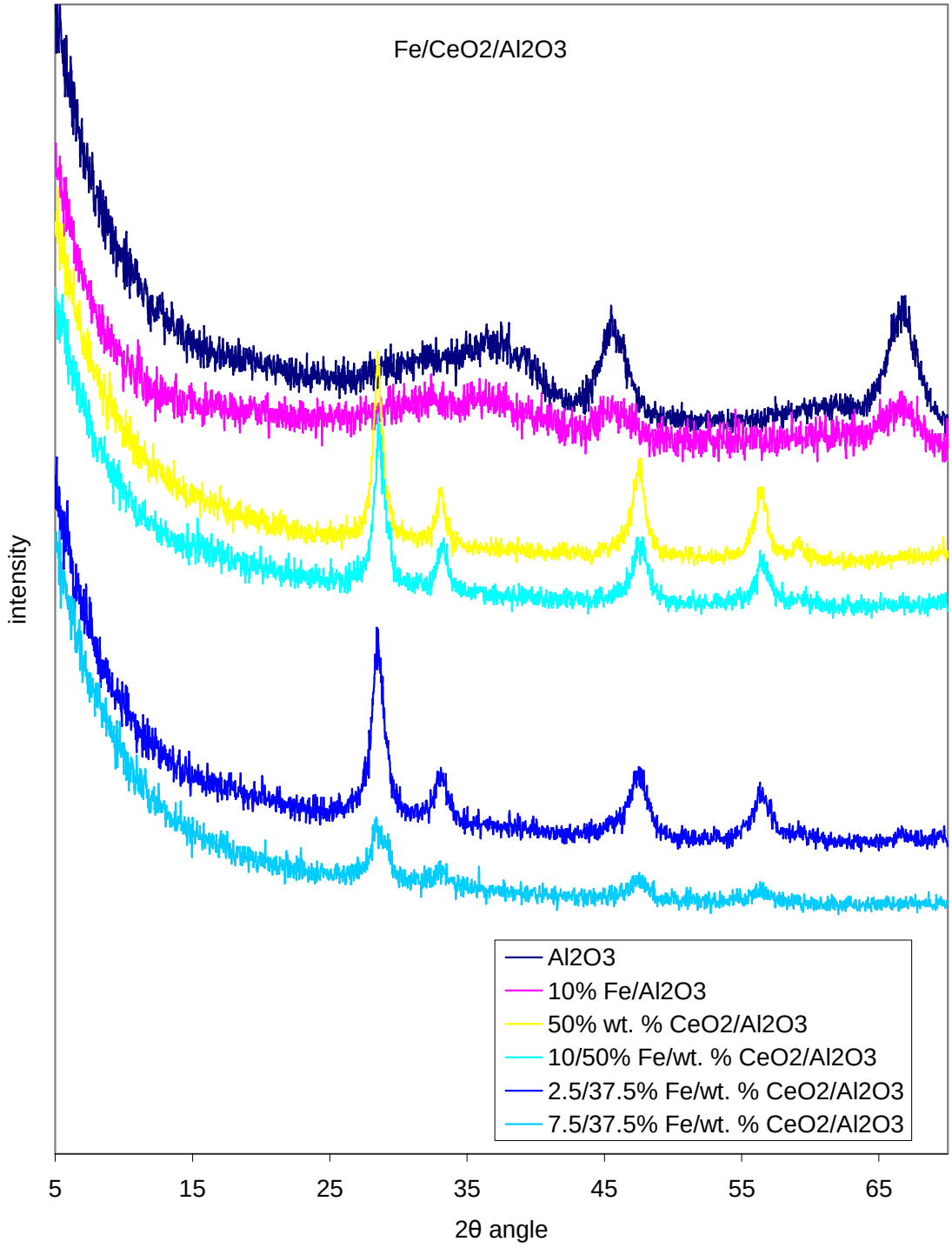

Figure 4.2. Comparison of XRD spectra for Fe on CeO_2/Al_2O_3 catalysts

As seen in Figure 4.1, there are no peaks observed for Fe on MgO/Al_2O_3 catalysts coded as MF2 and MF7. This shows a high dispersion of Fe on Al_2O_3 support. For the other catalysts, three major diffraction peaks of magnesium oxide can be seen at 2θ angles of 36.72, 42.67 and 62.12^o. Iron oxide phase was identified by its major peaks at 2θ angles of 44.35 and 64.53. XRD results of cerium promoted catalysts show that there are no significant peaks observed for Fe on CeO_2/Al_2O_3 catalysts coded as FC2 and FC7, which are those having low CeO_2 and high Fe containing catalysts. And for other catalysts, the peaks emerged are the major peaks of CeO_2 at 28.55, 33.08, 47.49 and 56.35. Corresponding peaks for both CeO_2 and MgO containing catalysts are increased with increased promoter loadings. Furthermore, it is seen that with increased Fe loading, CeO_2 dispersion is also increased when FC8 and FC9 are compared. There were no peaks observed related for iron oxides in the catalysts, and it can be said that the sizes of crystallites are below 5 nm since XRD is insensitive to crystals below 5nm [Neimantsverdriet 2007].

Average crystallite size calculations show that the presence of Fe improves the dispersion of CeO_2 and MgO on alumina by reducing crystallite size from 11.7 to 5.7 nm for CeO_2 and from 34.1 to 28.7 nm for MgO as seen in Table 4.1 and 4.2. FeO crystalline phase was observed for only 2.5/37.5% $Fe/MgO/Al_2O_3$ and 7.5/37.5% $Fe/MgO/Al_2O_3$ catalysts.

Table 4.1. Average crystallite thicknesses and crystalline phases of the synthesized Fe on CeO_2/Al_2O_3 catalysts.

Catalyst code	**wt. % Fe on CeO_2/Al_2O_3**	**wt. % CeO_2**	**wt. % Al_2O_3**	**Average crystallite Thickness**	**Crystalline Phase**
CF1	0	0	100	6.8	Al_2O_3
CF2	10	0	90	-	-
CF3	0	50	50	11.7	CeO
CF4	10	50	40	5.7	CeO
CF5	5	25	70	<5nm	CeO
CF6	2.5	12.5	85	<5nm	CeO
CF7	7.5	12.5	80	-	-
CF8	2.5	37.5	60	11.4	CeO
CF9	7.5	37.5	55	<5nm	CeO

Table 4.2. Average crystallite thicknesses and crystalline phases of the synthesized Fe on MgO/Al_2O_3 catalysts.

Catalyst code	**wt. % Fe on MgO/Al_2O_3**	**wt. % MgO**	**wt. % Al_2O_3**	**Average crystallite Thickness**	**Crystalline Phase**
MC1	0	0	100	6.8	Al_2O_3
MC2	10	0	90	-	-
MC3	0	50	50	34.1 28.3	MgO FeO
MC4	10	50	40	-	MgO
MC5	5	25	70	<5nm	-
MC6	2.5	12.5	85	<5nm	Fe
MC7	7.5	12.5	80	11.4 12.3	Fe
MC8	2.5	37.5	60	7.5 11.6 6.8	Fe MgO
MC9	7.5	37.5	55	- 34.1	Fe MgO

Porosity and the specific surface area of some oxide samples are evaluated by using Brunauer-Emmett-Teller (BET) method and Micrometrix Gemini V instrument operated in the scan mode. The surface areas of the catalysts are given in Table 4.3 and 4.4. The surface area decreased with increased loading of both CeO and Fe on Al_2O_3 for CeO/Al_2O_3 catalysts as expected. But MgO/Al_2O_3 catalysts showed a different behaviour. Their surface areas were high at the low and high loadings whereas at moderate loadings, the surface area was low. Furthermore, it is observed that when CeO loading levels are low, surface area increased with decreased Fe loadings, yet a completely different behaviour was observed when CeO loadings were high; in fact, the surface area slightly increased with increased Fe loadings. These behaviours can be seen in Figure 4.3.

Table 4.3. BET Results of synthesized Fe on $CeOO/Al_2O_3$ catalysts.

Catalyst code		**Wt. % Fe**	**wt. % CeO_2**	**wt. % Al_2O_3**	**BET Surface Area (m^2/g)**
CF1	Al_2O_3	0	0	100	190.63
CF2	10% Fe/Al_2O_3	10	0	90	187.68
CF3	50% CeO/Al_2O_3	0	50	50	129.46
CF4	10/50% $Fe/CeO/Al_2O_3$	10	50	40	99.44
CF5	5/25% $Fe/CeO/Al_2O_3$	5	25	70	161.56
CF6	2.5/12.5% $Fe/CeO/Al_2O_3$	2.5	12.5	85	174.42
CF7	7.5/12.5% $Fe/CeO/Al_2O_3$	7.5	12.5	80	169.34
CF8	2.5/37.5% $Fe/CeO/Al_2O_3$	2.5	37.5	60	136.68
CF9	7.5/37.5% $Fe/CeO/Al_2O_3$	7.5	37.5	55	135.13

Table 4.4. BET Results of synthesized Fe on MgO/Al_2O_3 catalysts.

Catalyst code		**wt. % Fe**	**wt. % MgO**	**wt. % Al_2O_3**	**BET Surface Area (m^2/g)**
MF1	Al_2O_3	0	0	100	190.63
MF2	10% Fe/Al_2O_3	10	0	90	187.68
MF3	50% MgO/Al_2O_3	0	50	50	175.23
MF4	10/50% $Fe/MgO/Al_2O_3$	10	50	40	189.03
MF5	5/25% $Fe/MgO/Al_2O_3$	5	25	70	166.51
MF6	2.5/12.5% $Fe/MgO/Al_2O_3$	2.5	12.5	85	182.27
MF7	7.5/12.5% $Fe/MgO/Al_2O_3$	7.5	12.5	80	173.43
MF8	2.5/37.5% $Fe/MgO/Al_2O_3$	2.5	37.5	60	142.73
MF9	7.5/37.5% $Fe/MgO/Al_2O_3$	7.5	37.5	55	174.79

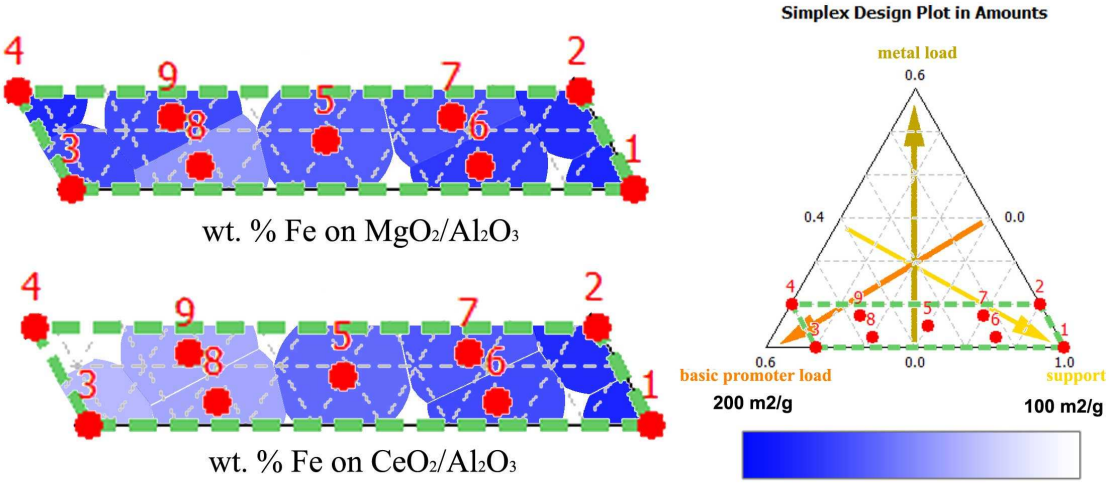

Figure 4.3. Specific surface area of catalysts.

FTIR spectral features of CO_2 adsorbed catalysts are shown in Figure 4.4 and Figure 4.5. CO_2 exposed catalysts showed strong bands that appeared at 1535 and 1410 cm^{-1}. These bands are assigned to surface inorganic carboxylate formed by adsorption of CO_2 at metal cations (Li 1989, Scmal 1998). 1652 cm^{-1} correspond to stretching vibration of O–H bond of the physically adsorbed water on the samples. FTIR spectra of CeO containing samples shows bands at 885 and 800 cm^{-1} unlike MgO containing

samples and also pure Al_2O_3 and Fe/Al_2O_3 catalysts. These bands correspond to the out of plane vibration of the carbonate CO_3^{2-} group [Li 1989].

Examining of the used catalysts shows that a new group of bands occurs at 1115, 1050, 1000, 930 and 870 cm^{-1} for 10% Fe/Al_2O_3 and 10/50% $Fe/CeO/Al_2O_3$ catalysts. First three peaks correspond to C–O stretch and the later two corresponds to aromatic C – H out-of-plane bending (Coates 2000). 10% Fe/Al_2O_3 also exhibits a double peak at 2950 and 2895 cm^{-1}. These twin peaks are also observed for 10/50% $Fe/CeO/Al_2O_3$ catalyst. Peak is found at 2950 cm^{-1} due to symmetric stretch of $–CH_3$ group and peak at 2895 cm^{-1} indicating polyatomic C_n-H-O entitles with C bonded to two or three H. Apart from these observations, weak methyl C – H asym./sym. bending with a very sharp peak was observed at 1380 cm^{-1} for used 7.5/37.5% $Fe/CeO/Al_2O_3$ catalyst (Coates 2000).

Similar to the CO_2 adsorption studies, NH_3 adsorption was also evaluated to observe acidic sites and shown in Figure 4.6 and 4.7. It is known that for all the mixed oxides, the characteristic bands of physically adsorbed NH_3, as coordinative bonded NH_3, and NH_4^+, each of which can be detected by means of their absorption bands [Tanabe 1989] but there are no bands related to acidic sites.

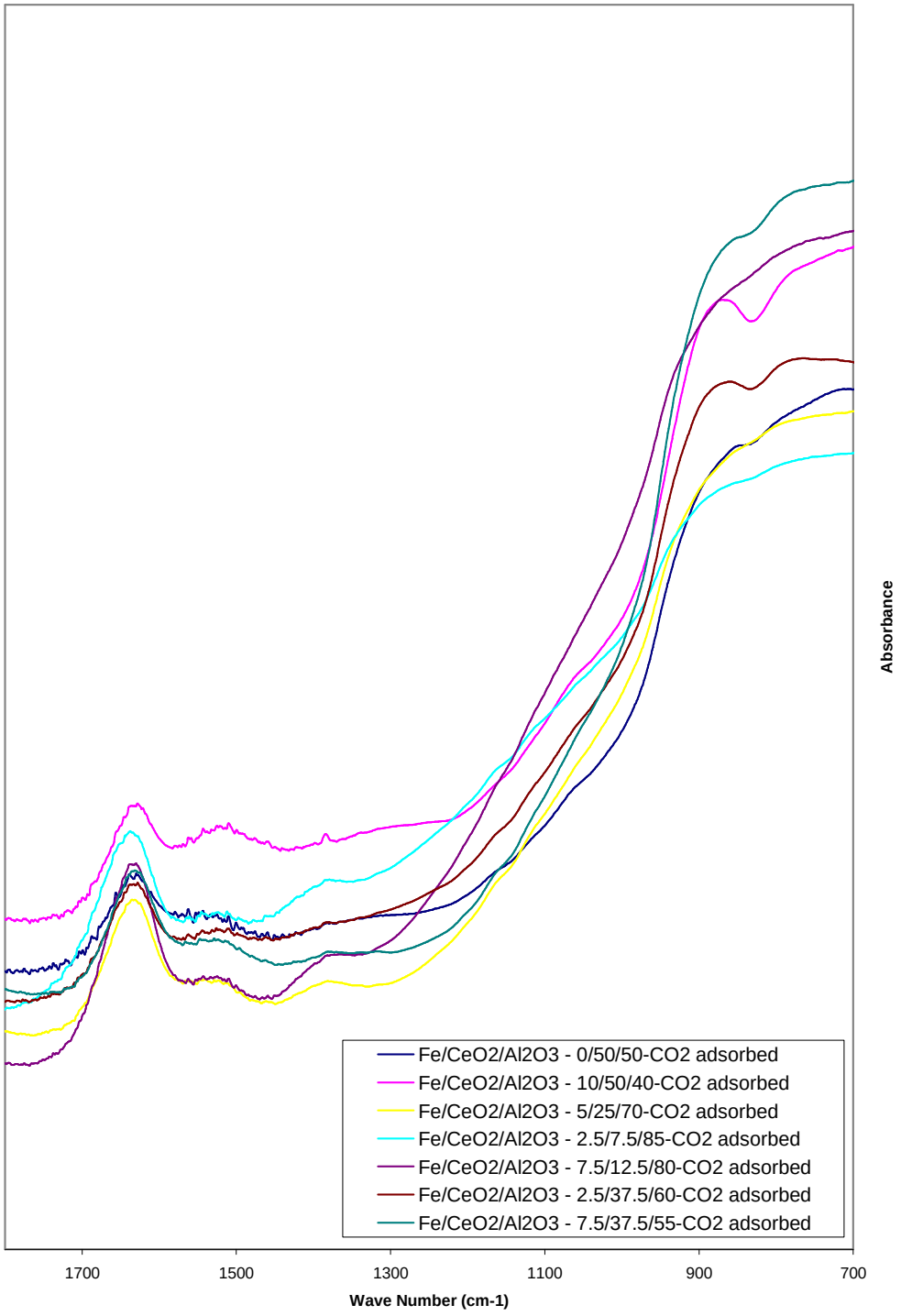

Figure 4.4. FTIR spectra of CO_2 adsorbed Fe on CeO_2/Al_2O_3 catalysts.

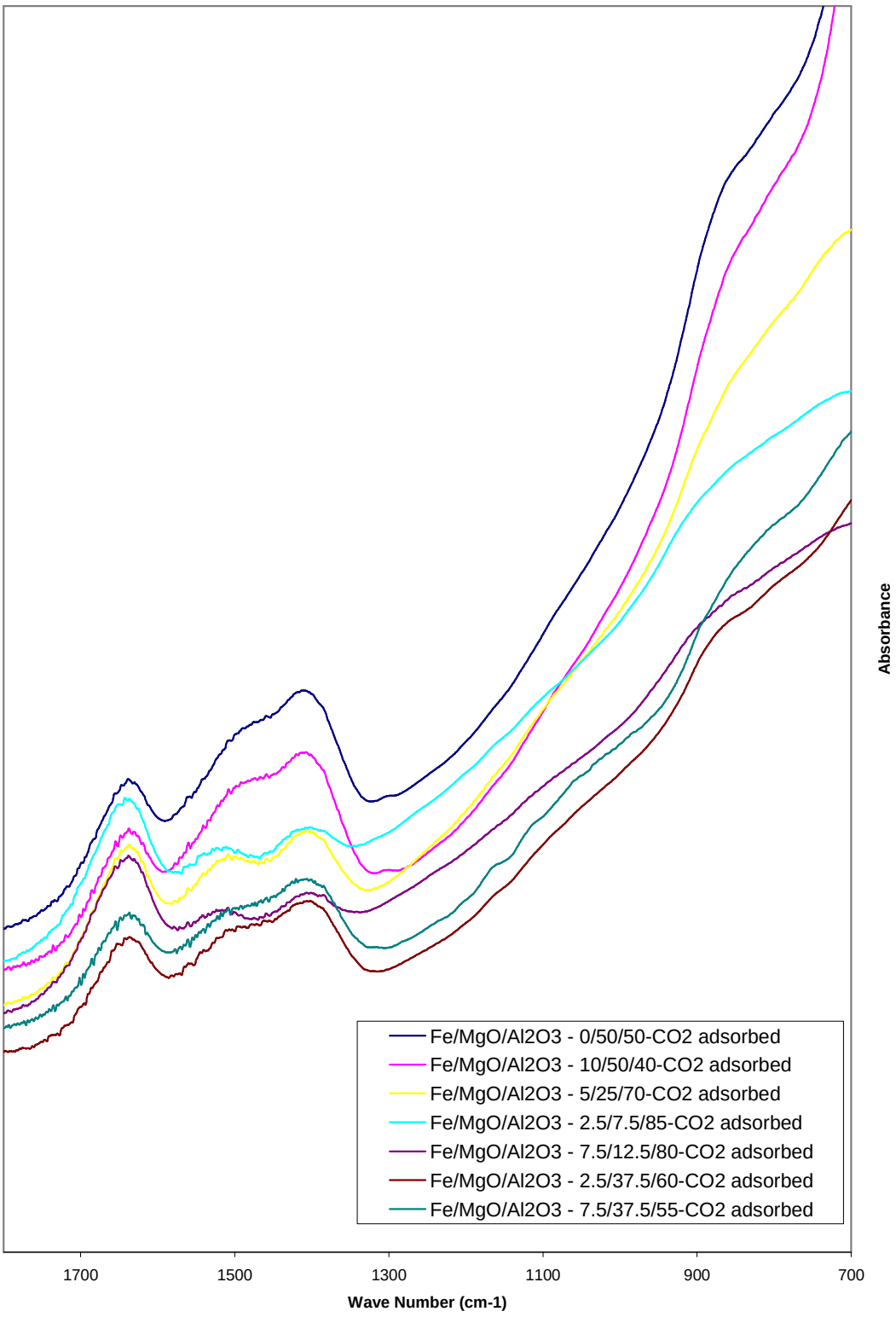

Figure 4.5. FTIR spectra of CO_2 adsorbed Fe on MgO/Al_2O_3 catalysts

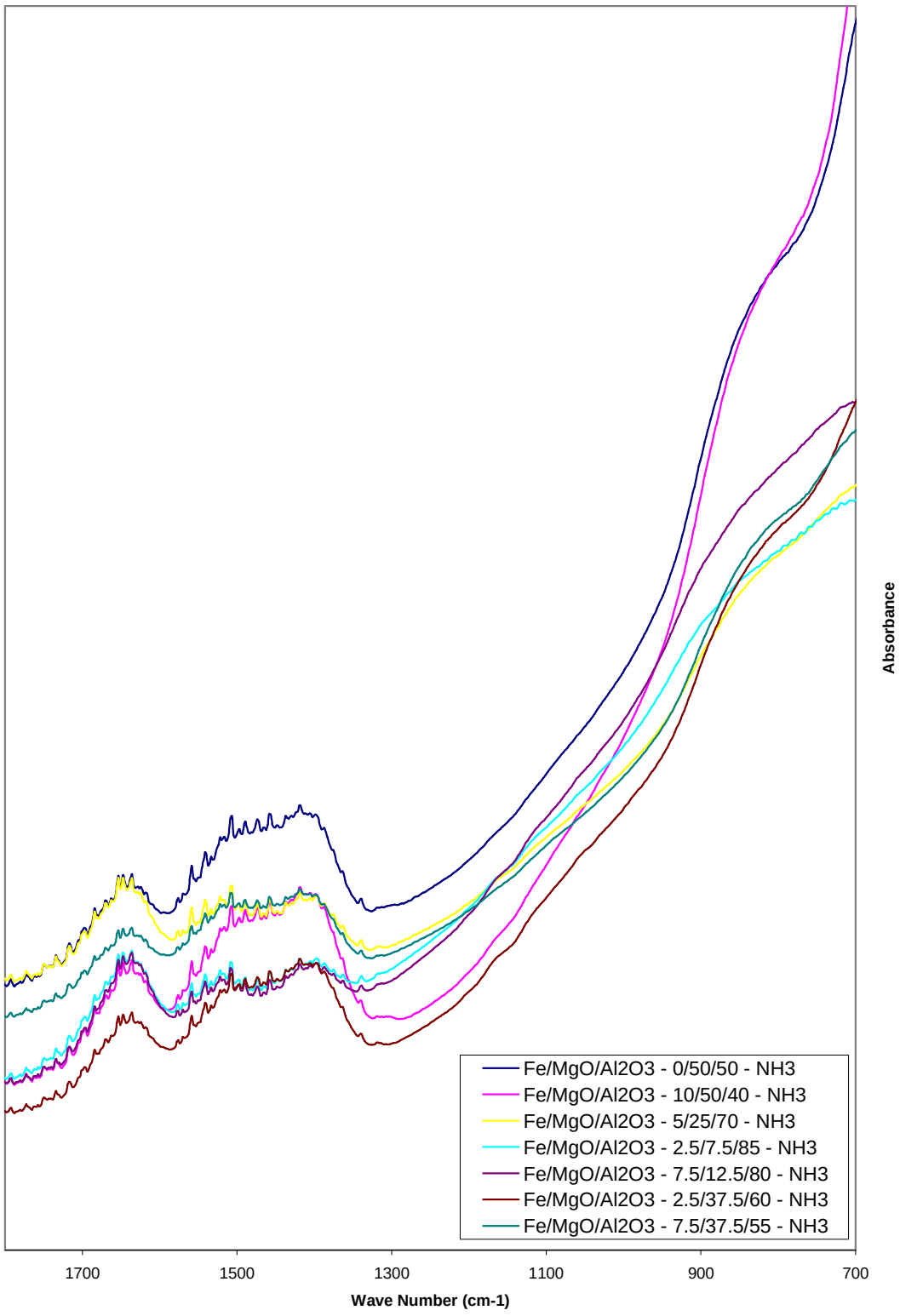

Figure 4.6. FTIR spectra of HNO_3 adsorbed Fe on MgO/Al_2O_3 catalysts.

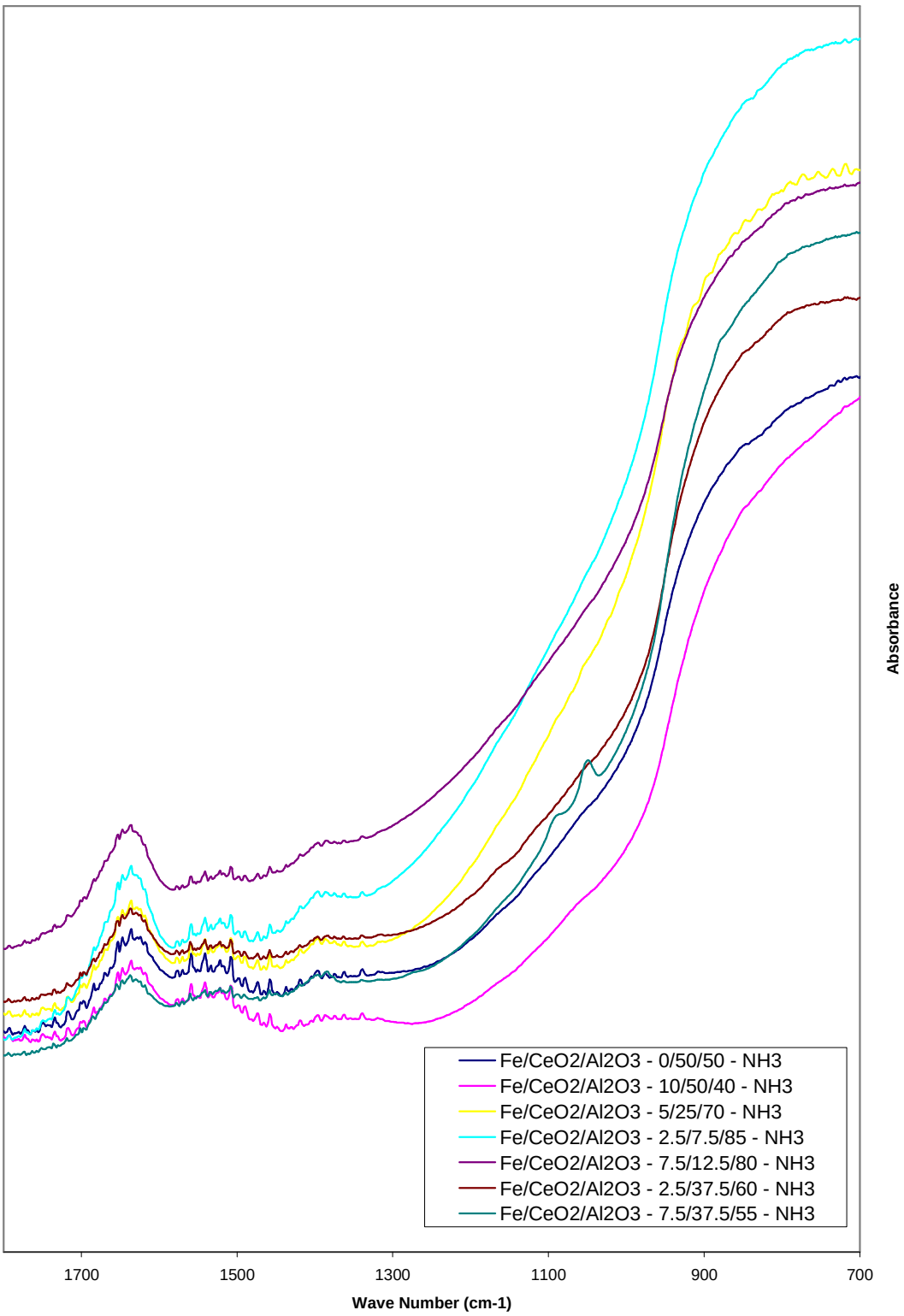

Figure 4.7. FTIR spectra of HNO_3 adsorbed Fe on CeO_2/Al_2O_3 catalysts.

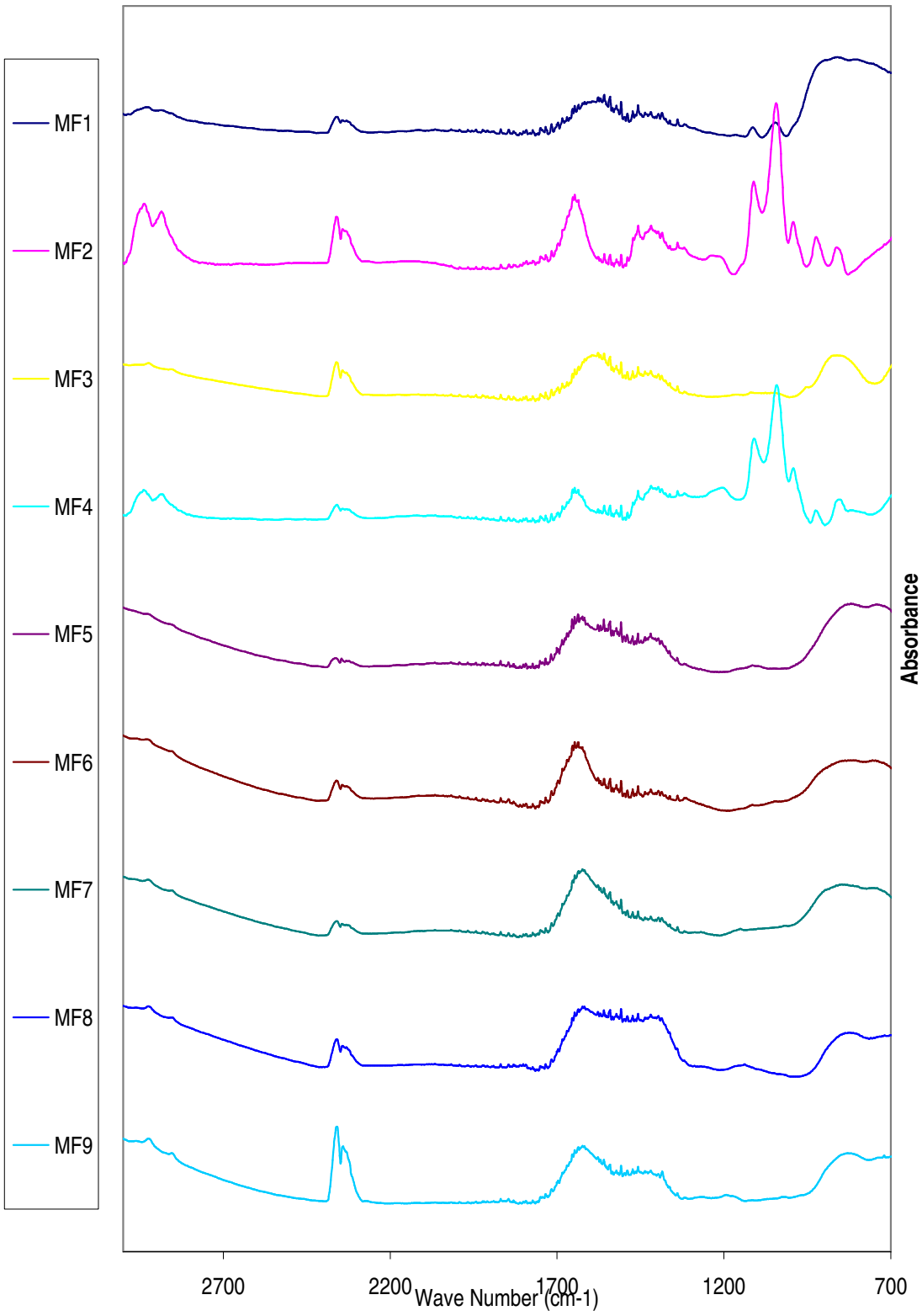

Figure 4.8. FTIR spectra of used Fe on MgO/Al_2O_3 catalysts.

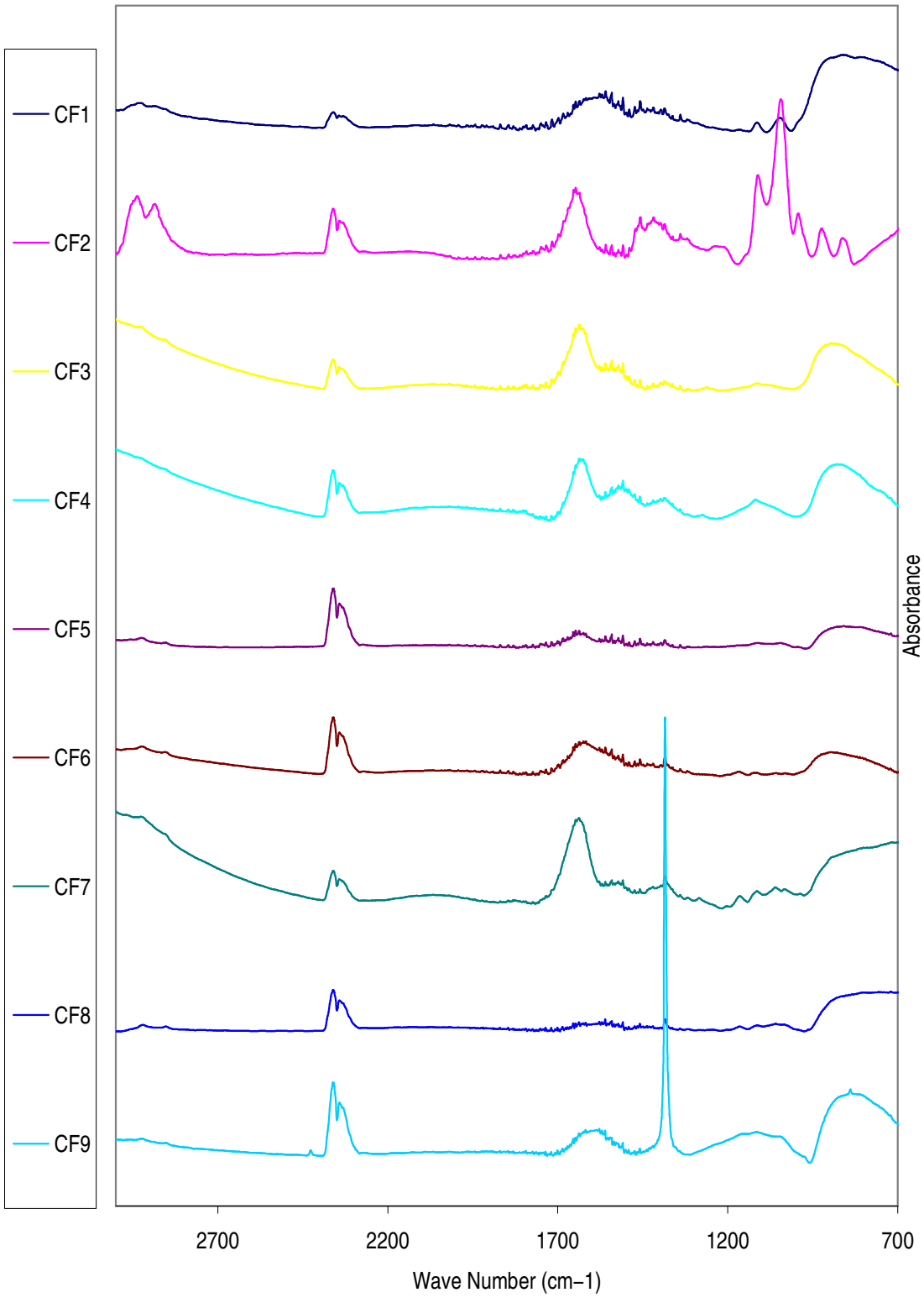

Figure 4.9. FTIR spectra of used Fe on CeO_2/Al_2O_3 catalysts.

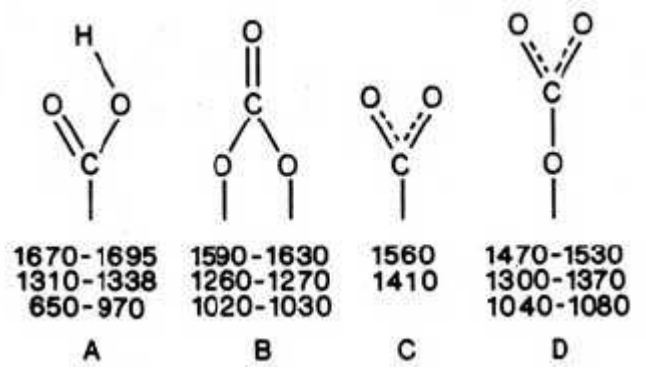

Figure 4.10. Assignment of carbonate-like species
(Source Jin 1987).

Total basicities and basic sites determined using CO_2 adsorption studies are given below in Figure 4.11 and Tables 4.5 and 4.6. Results show that for MgO catalysts total basic sites increased with increased MgO loadings and slightly decreased with increased Fe loadings. A completely different behaviour was observed for the CeO_2 containing catalysts. Low loadings of CeO_2 and high loadings of Fe results in high number of basic sites and a sharp decrease was observed in the absence of CeO_2. Peaks at 1400 and 1535 cm^{-1} corresponds to inorganic carboxylate [Schmal 1998]. Furthermore, CeO_2 promotes the formation of two peaks at 885 and 800 cm^{-1}. This site contributes to unidendate carbonate [Jin 1987, Onashi 1989]. The addition of Fe to CeO_2 catalyst is also shifted to the band observed at 865 cm^{-1} to 885 cm^{-1} resulting in stronger basic sites. A similar effect was observed for when MgO containing catalysts compared to pure Al_2O_3 and Fe/Al_2O_3 catalysts. Band observed at 1400 cm^{-1} shifted to 1410 cm^{-1} in the presence of MgO resulting in a stronger basic site [Coates 2000].

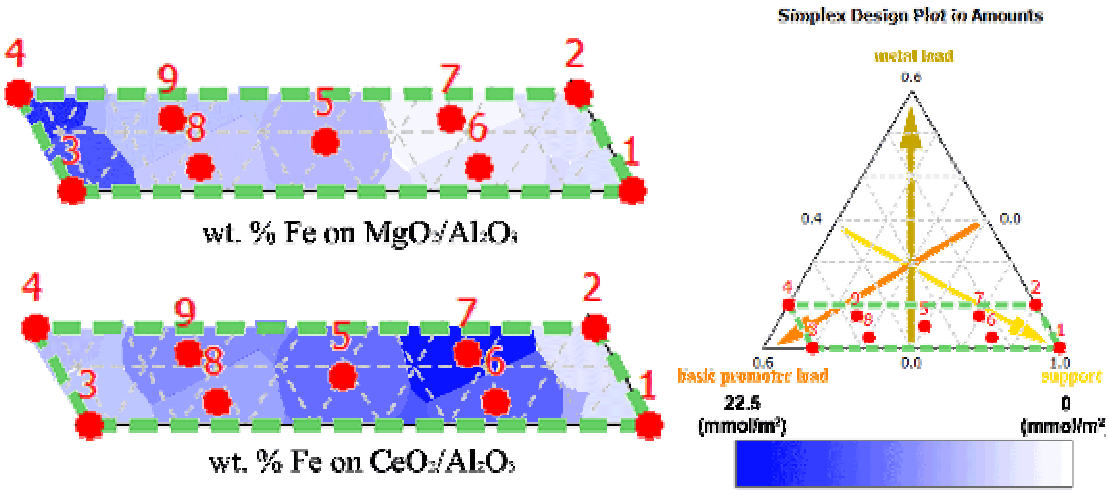

Figure 4.11. Total Basicity of surface area of catalysts.

Table 4.5. Basicity of synthesized Fe on CeO/Al_2O_3 catalysts.

	Peak wave-number (cm^{-1})				**Basicity ($mmol/m^2$)**		
sample name	**Inorganic carboxylate site**		**Unidentate carbonate site**		**Inorganic carboxylate site**	**Unidentate carbonate site**	**Total**
CF1	1535	1400	-	-	2.82	0.00	2.82
CF2	1535	1400	-	-	2.74	0.00	2.74
CF3	1535	1400	865	800	2.28	3.42	5.70
CF4	1535	1400	885	800	1.54	4.56	6.10
CF5	1535	1400	885	800	5.18	8.25	13.43
CF6	1535	1400	885	800	5.54	9.29	14.83
CF7	1535	1400	885	800	10.01	12.49	22.50
CF8	1535	1400	885	800	1.32	7.21	8.52
CF9	1535	1400	885	800	2.26	8.42	10.69

Table 4.6. Basicity of synthesized Fe on CeO/Al_2O_3 catalysts.

	Peak wave-number (cm^{-1})		**Basicity ($mmol/m^2$)**
sample name	**Inorganic carboxylate site**		**Inorganic carboxylate site**
MF1	1535	1400	2.82
MF2	1535	1400	2.74
MF3	1535	1410	16.22
MF4	1535	1410	19.68
MF5	1535	1410	6.69
MF6	1535	1410	2.46
MF7	1535	1410	1.19
MF8	1535	1410	5.51
MF9	1535	1410	5.82

4.2. Catalyst Testing

Catalysts testing set up is prepared as shown in Figure 4.4 and tested for leaks. All flow lines are heated to prevent the condensation of reactants/products. Outlet stream is first fed to three serially connected washing bottles to remove liquid products. Then, the stream passed through a Nafion membrane further to remove water from the stream before GC analysis of the gas stream. The dried gas stream was analyzed in 1 h intervals to determine if steady state was reached. After the system reached the steady state, the liquid and gas streams were evaluated using GCs.

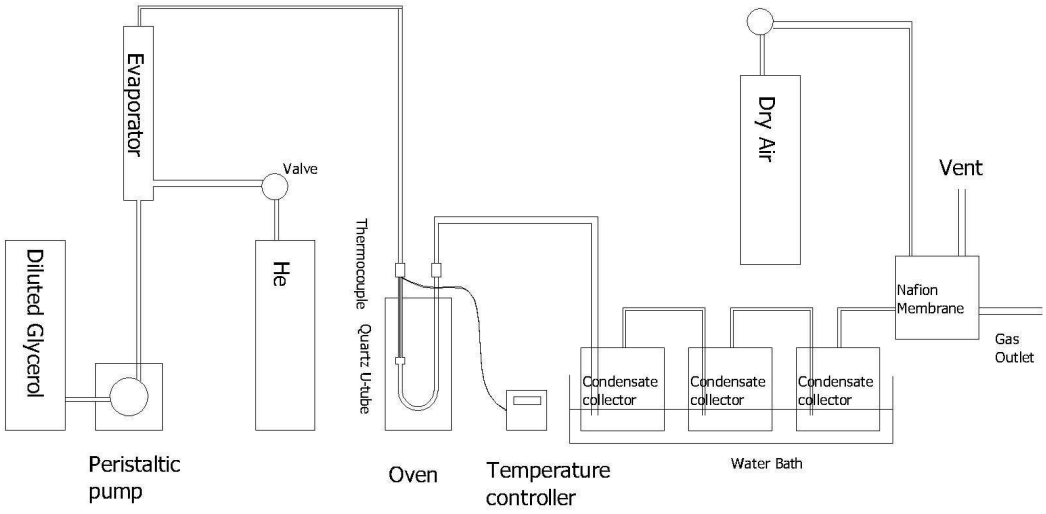

(a)

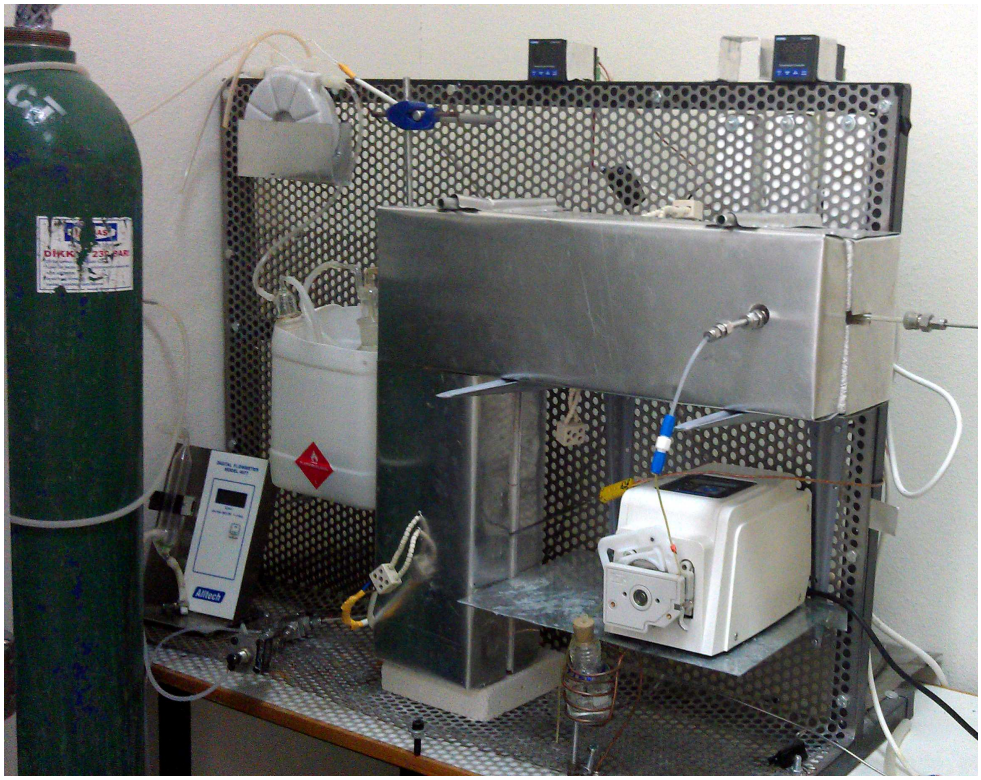

(b)

Figure 4.12. (a) Schematic of the glycerol steam reforming system, (b) constructed catalyst testing setup.

The analysis of liquid products of the blank tests, i.e. no catalyst in the reactor, shows that conversion to gaseous products are observed 53%, 45%, 43% and 40%, respectively for reactor temperatures 350, 400, 450 and 500 ºC for 3 water/glycerol molar ratio. These results are also similar with the only study reported blank run conversions; Chiodo et al used higher temperatures up to 800 ºC and they reported gaseous product formation [Chiodo 2010]. It is observed that the percentage of liquid products slightly increased with increased temperature at this molar ratio. Catalyst tests are evaluated for the temperatures 400, 450 and 500 ºC considering possible reforming that can occur at relatively low temperature 350 ºC. A representative gas chromatograms of gas stream analysis obtained for $Fe/CeO_2/Al_2O_3$ with loadings of 7.5, 37.5 and 55% is given in Figure C.1. in Appendix C. CO and CO_2 are the only detected gases in the gas stream and % Carbon Selectivity to CO and CO_2 and total gaseous products was calculated as;

$$\text{CO Selectivity} = \frac{\text{CO in the gaseous products}}{3 \text{ x Glycerol converted}} x100\% \quad (4.1)$$

$$\text{CO}_2 \text{ Selectivity} = \frac{\text{CO}_2 \text{ in the gaseous products}}{3 \text{ x Glycerol converted}} x100\% \quad (4.2)$$

$$\text{Gaseous Product Selectivity} = \frac{\text{CO}_2 \text{ in the gaseous products} + \text{CO in the gaseous products}}{3 \text{ x Glycerol converted}} x100\% \quad (4.3)$$

Gas phase products and the required glycerol and water to form these products are used to determine H_2 in the gas phase. And selectivity and % yield calculated as;

$$\text{H}_2 \text{ Selectivity} = \frac{\text{H}_2 \text{ in the Gas Phase}}{\text{Total Carbon coverted to the Gas Phase}} \quad (4.4)$$

$$\%\text{H}_2 \text{ Yield} = \left(\frac{\text{Actual yield}}{\text{Theoretical Yield}} \text{x}100\right) \quad (4.5)$$

Here theoretical yield is the ratio of H_2 to total carbon feed for complete conversion of hydrogen atoms in the feed to H_2 molecule.

In order to investigate the influence of support properties on the steam reforming iron oxide particle sizes was kept relatively the same and was below 5 nm. Similarly, both CeO_2 and MgO crystallites were about 5 nm or below. The results in Table 4.7 and 4.8 are summarized in Figure 4.14 and 15 for all the catalysts and temperatures. MF4, 10/50% Fe/MgO/Al_2O_3, catalyst shows high gaseous product selectivity at all temperatures. When MF4, 10/50% MgO/Al_2O_3, catalyst was considered, the gaseous product selectivity was compared to CF4, 10/50% CeO_2/Al_2O_3, catalyst. This can be attributed to possible reaction path for formation of CO which is dehydrogenation of alcohol accompanied by the dehydration of alcohols over basic oxides through reaction path (1) rather than (19) or (20) shown in Figure 4.13. Since basicity is more dominant on Fe promoted catalysts than CeO_2 promoted catalysts (Tanabe1989), MF4 has higher basicity than CeO_2. Yet the analysis on CF4 catalyst shows that there is no CO formation while CO_2 was the only observed gas products and its concentration stayed constant with temperature increase.

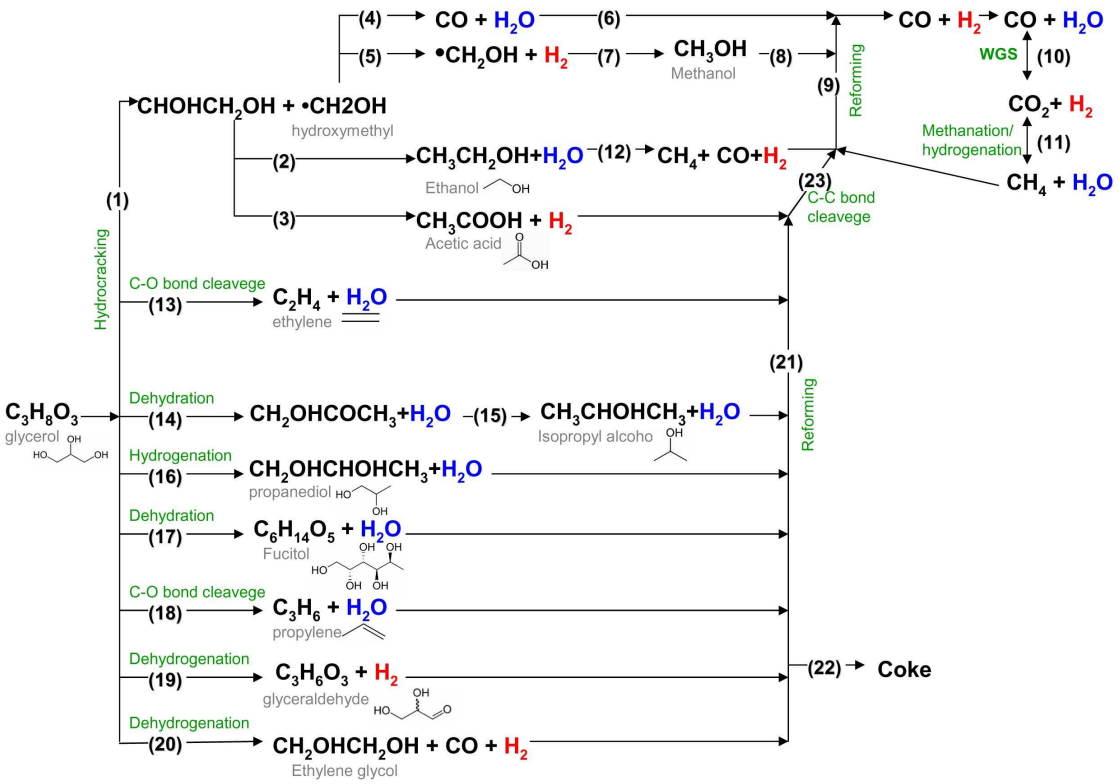

Figure 4.13: Main reaction pathways in occur in hydrogen production from glycerol by steam reforming (Source: Adhikari 2009, Somoraj 1994, Xiao 2008).

Selectivity of gaseous products is given in Table 4.7 and 4.8 for MgO and CeO_2 containing catalysts, respectively. MgO catalysts show decreasing activity behaviour with decreased MgO loadings but increased temperatures. The main reason behind this behaviour is that total basicity of the catalyst is increased with increased MgO loading. This increase in basicity is linked with the increase in number of basic OH groups on $A1_2O_3$ due to the addition of MgO (Tanabe 1989), and results in better performance of catalyst for hydrogenolysis. Furthermore it prevents serious coke formation mostly observed on MgO based catalysts by promoting the reaction paths leading C-C bond cleavage rather than C-O bond cleavage (Tanabe 1989). FTIR observations on used catalysts shows that no C-C bands supports this claim and hence, the catalyst prevents the reaction path (22) as shown in Figure 4.13 which leads to coke formation. Another reason of low coke formation is that large molecules like Fuctiol require promoting acidic sites for dehydration of glycerol through reaction path (17) in Figure 4.13 (Tanabe 1989). Since none of the prepared catalysts shows any observable acidic sites, this reaction path is not favourable on the prepared catalyst in this study.

High activity toward water gas shift reaction (WGS), path (10) and (11), results in high conversion of intermediate CH_4 product to CO_2, CO, H_2O and $H_{2;}$ thus, no detectable CH_4 observed in the gas streams. The activity of MF4 also shows significant product distribution due to its exothermic behaviour observed with increased temperature. At 400 ºC, CO/CO_2 ratio is 0.9 and as the temperature increases, this ratio increases two folds. This behaviour can be observed for all the catalysts. The selectivity of the catalysts decreases with temperature and remains constant for CO_2 and CO.

CeO_2 containing catalysts show better gaseous product selectivity at moderate loadings and their activities dropped sharply to the design extremes. This might be caused by interaction between CeO_2 and Fe on alumina. Another important result is low loadings of Fe on both CeO_2 and MgO containing catalysts show poor activity performances; in fact, it is worse than pure Al_2O_3. All these catalysts have broader and shorter XRD peaks. Although most of the catalysts are XRD amorphous, these catalysts can have crystallite sizes smaller than 5 nm.

Infrared spectroscopy coupled with multivariate calibration was applied for the determination of glycerol, acetic acid and isoprophyl alcohol in the liquid products. Wavelength selection is applied to improve the predictive ability of multivariate calibration methods due to the complexity of the IR spectra and low absorbance values of samples (Özdemir 2006). Pure water is taken as background and noise regions are removed. Infrared spectroscopic measurements of the samples were carried out in diffuse reflectance mode between 600 and 4,000 cm^{-1} wave number interval and resolution was 1 cm^{-1}. A small set of wavelengths is selected from a full spectral data matrix and evolved to an optimum solution using a genetic algorithm applied to a number of wavelength selection problems. And multivariate calibration models were built for 70 samples and a separate set of spectra of 35 samples used for validation of the model. The GILS method was implemented in MATLAB programming language Version 7.0 (MathWorks Inc, Natick, MA) (Özdemir 2011). When standard error of calibration (SEC) and standard error of prediction (SEP) were inspected as given in Table 4.7, it ranges from 0.0015 to 0.0039 w/w%.

Table 4.7. Overall, standard error of calibration (SEC) and standard error of prediction (SEP) values for models build by multivariate calibration.

	Glycerol	**Isopropyl Alcohol**	**Acetic Acid**
SEP (w/w%)	0.021	0.015	0.039
SEC (w/w%)	0.015	0.008	0.015

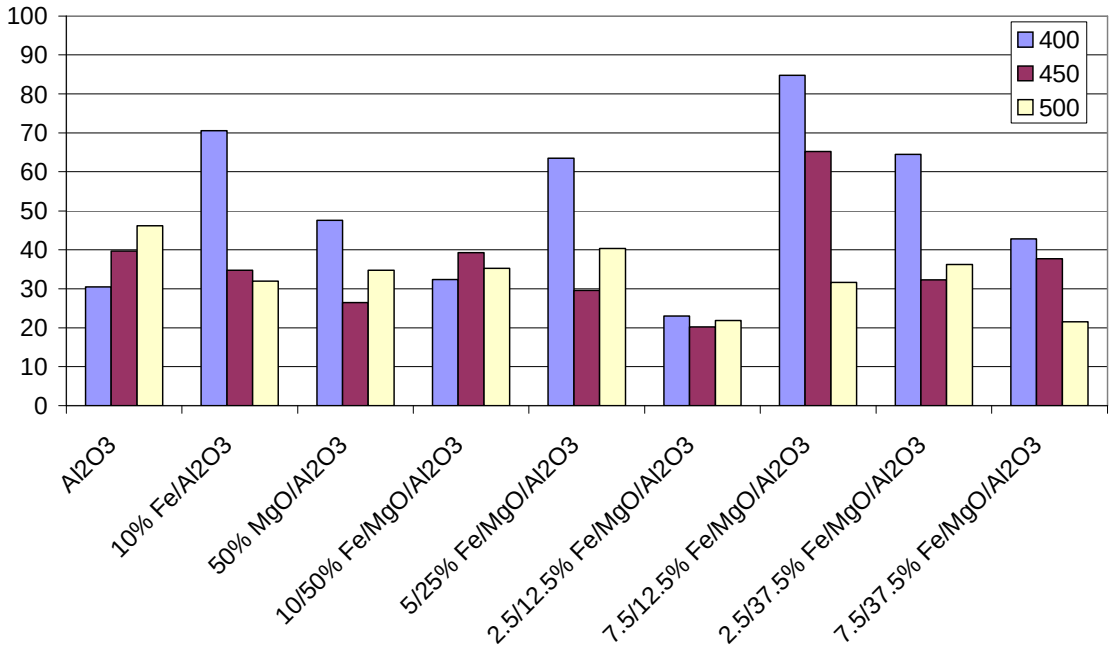

Figure 4.14. w/w% amounts of glycerol in liquid products for MgO modified catalysts.

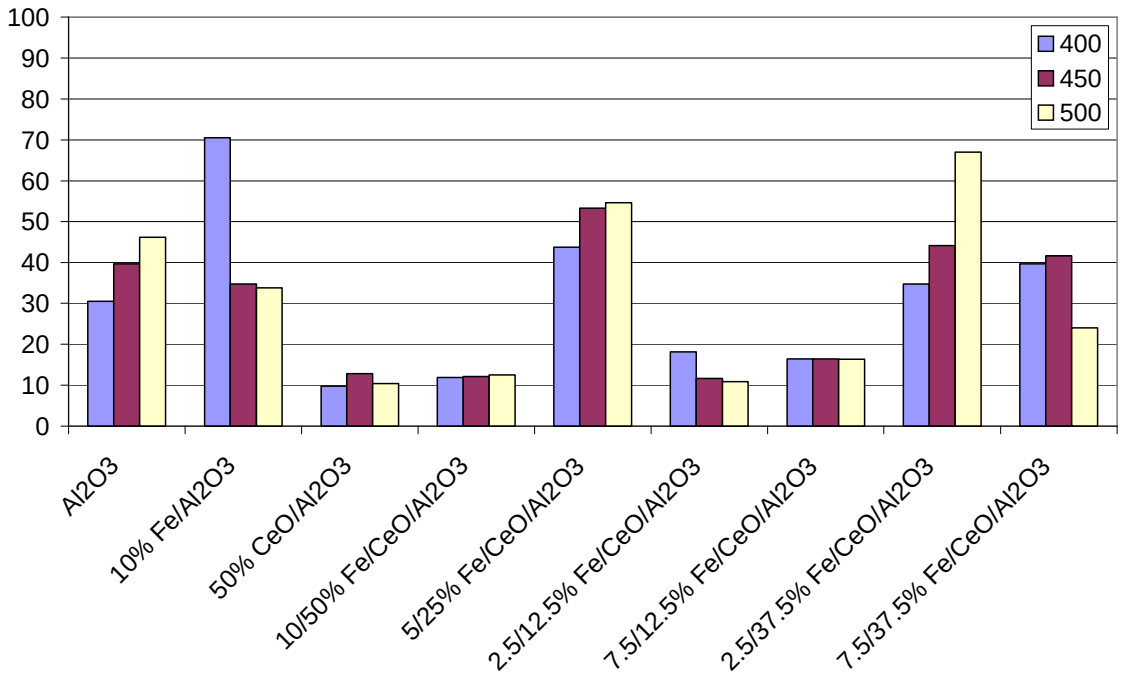

Figure 4.15. w/w% amounts of glycerol in liquid products for CeO_2 modified catalysts.

FTIR studies shows that none or negligible amounts of isopropyl alcohol or acetic acid exists in all liquid products. Glycerol concentration in the samples, on the other hand, decreases with increased temperatures for MgO modified catalysts, as seen in Table 4.9. CeO_2 modified catalysts with high loadings shows a significantly lower glycerol content in the liquid phase. And the catalysts with loadings 5/25 % Fe/ CeO_2/Al_2O_3 and 2.5/37.5 % Fe/ CeO_2/Al_2O_3 shows a different behaviour compared to other catalysts, as given in Table 4.10. Their glycerol contents are increased with the increased temperature. It is known that other liquid products acetaldehyde (Güemez 2010), prophylene glycol and ethylene glycol (Güemez 2008) can form during the reaction.

GC-MS results of the liquid products show various fragments of carbonaceous species. It is observed that GC-MS used in this study cannot separate CO from N_2 and C_2H_4; thus, quantitative analysis could not be carried on with GC-MS as seen in Table 4.8. The major species observed are also similar with those reported in the literature [Chiodo 2010]. It is reported that glycerol decomposes to the formation of CO, CO_2, olefins, water, hydrogen, acetone, acetaldehyde, ethanol, propanol, acetic acid and 2,3-dyhydroxylpropanal at high temperatures.

Table 4.8 Mass fragments detected by GC-MS in liquid phase. (●) mass detected with significant intensity over ($2x10^5$ intensity in $8x10^6$), (○) mass detected insignificantly, (-) not detected.

		Temperature		
Fragment Mass	**Fragments**	**400**	**450**	**500**
14	CH_2	●	●	●
18	H_2O	●	●	●
28	CO, C_2H_4	●	●	●
32	CH_4O	●	●	●
34	H_2O_2	●	○	●
37	C_3H	○	○	○
39	C_3H_3	-	-	●
45	CH_3CHOH, CH_2CH_2OH, CH_2OCH_2	●	○	○
57	$C_2H_5C=O$	○	○	●

Table 4.9. % mass of detected compounds in both gaseous and liquid outlet streams (% analysis error % ± 5.6.

	Glycerol (%)	**Acetic acid** (%)	**Isoropyl alcohol** (%)	**MeOH** (%)	**EtOH** (%)	**CO** (%)	**CO_2** (%)	**Total** (%)
Blank	79	0	0	5	16	0	0	100
Al_2O_3	12	0	0	1	7	8	13	41
10% Fe/Al_2O_3	32	0	0	17	33	5	12	98
50% CeO/Al_2O_3	0	0	0	0	0	0	30	31
7.5/37.5% Fe/CeO/Al_2O_3	25	0	0	4	20	0	33	81
50% MgO/Al_2O_3	10	0	0	4	69	5	13	100
2.5/37.5% Fe/MgO/Al_2O_3	39	0	0	8	29	9	16	100

Liquid product analysis of GC analysis shows that at 400 ºC, no formaldehyde or ethylene glycol was observed for any of the catalysts as seen in Table 4.9. Yet, the blank runs show that glycerol composes to ethanol (EtOH) and many trace hydrocarbons at this temperature. The presence of Al_2O_3 results in the absence of trace hydrocarbons but EtOH is the only liquid product that can be detected. MeOH formation is due to C–C bond cleavage when the high amounts of Fe loaded on the support was observed from the liquid phases of 10% w/w Fe/Al_2O_3 and 10/50% w/w $Fe/MgO/Al_2O_3$. When basic supports were compared, it was observed that only trace amounts of EtOH and MeOH were observed on 50% w/w CeO_2/Al_2O_3 as compared to EtOH observed in liquid phase analysis of liquid products analysis of 50% w/w CeO_2/Al_2O_3. Liquid products were composed of many undetermined trace components for Al_2O_3 and CeO_2/Al_2O_3 catalysts. These products results from C–OH bond cleavage hindered with the presence of Fe and MgO on the catalysts. Thus, it can be concluded that the presence of unidentate carbonate sites do not facilitate for C–C bond cleavage but rather improves WGS performance. C–C bond cleavage mainly corresponds to inorganic carboxlate site observed for both MgO and CeO_2 containing catalysts. And the presence of Fe promotes C–OH bond cleavage and a limited C–C bond cleavage. Also increased crystallite size results in increase in both of these bond cleavages.

Table 4.10. Selectivity of gaseous products over total carbon feed for $Fe/MgO/Al_2O_3$ catalysts

	% Selectivity CO			**% Selectivity CO_2**			**% Selectivity Gaseous Products**		
Catalyst\Temperature (ºC)	**400**	**450**	**500**	**400**	**450**	**500**	**400**	**450**	**500**
Al_2O_3	10	8	5	11	12	14	21	20	18
10% Fe/Al_2O_3	13	3	15	21	13	9	34	16	24
50% MgO/Al_2O_3	21	6	3	15	11	13	36	16	16
10/50% $Fe/MgO/Al_2O_3$	14	25	21	15	10	9	29	35	30
5/25% $Fe/MgO/Al_2O_3$	13	6	9	24	12	12	37	18	21
2.5/12.5% $Fe/MgO/Al_2O_3$	0	0	0	10	10	8	11	10	8
7.5/12.5% $Fe/MgO/Al_2O_3$	10	2	0	23	20	21	33	21	21
2.5/37.5% $Fe/MgO/Al_2O_3$	13	4	4	20	10	12	33	14	16
7.5/37.5% $Fe/MgO/Al_2O_3$	4	8	0	14	15	10	19	23	10

Table 4.11. Selectivity of gaseous products over total carbon feed for $Fe/CeO_2/Al_2O_3$ catalysts.

	% Selectivity CO			% Selectivity CO_2			% Selectivity Gaseous Products		
Catalyst\Temperature (°C)	**400**	**450**	**500**	**400**	**450**	**500**	**400**	**450**	**500**
Al_2O_3	4	3	1	4	4	4	8	7	5
10% Fe/Al_2O_3	4	1	1	6	4	4	9	6	6
50% CeO/Al_2O_3	0	0	0	4	4	4	4	5	4
10/50% $Fe/CeO/Al_2O_3$	0	0	0	5	5	5	5	5	5
5/25% $Fe/CeO/Al_2O_3$	4	0	16	7	5	5	11	5	21
2.5/12.5% $Fe/CeO/Al_2O_3$	0	0	0	5	5	4	5	5	4
7.5/12.5% $Fe/CeO/Al_2O_3$	0	0	0	6	6	6	6	6	6
2.5/37.5% $Fe/CeO/Al_2O_3$	5	7	13	8	7	8	13	14	22
7.5/37.5% $Fe/CeO/Al_2O_3$	0	9	0	6	7	7	6	16	7

Gaseous product analysis shows that for all the catalysts, methanation was not observed and the conversions to CO and CO_2 are given in Tables 4.10 and 4.11. It is observed that the catalysts promote the conversion of glycerol at low temperatures on all the catalysts. The activity tests show that the presence of Fe promotes glycerol conversion and gas product selectivity for MgO supported catalysts when similar glycerol conversions were compared. 10% Fe/Al_2O_3 catalyst shows lower glycerol conversion but higher gas product selectivity, as compared to MgO and CeO_2 modified catalyst. This result indicates the ability of Fe to promote dehydrogenation followed by C–C bond cleavage which results in CO_2 formation [Somoraj 1994]. A similar behaviour was observed for the catalysts with higher basicity or the presence of monodentate carbonate basic sites. Also, CO formation was hindered but CO_2 formation was favoured for CeO_2 promoted catalysts having unidentate carbonate basic sites. This also results in high activity of steam reforming. In literature, mostly the effect of total basicity is observed rather than the effect of type of basic site [Wan 2008, Buffoni 2009]. The addition of Fe to CeO_2 supported catalysts does not change glycerol conversion or gaseous product selectivity significantly.

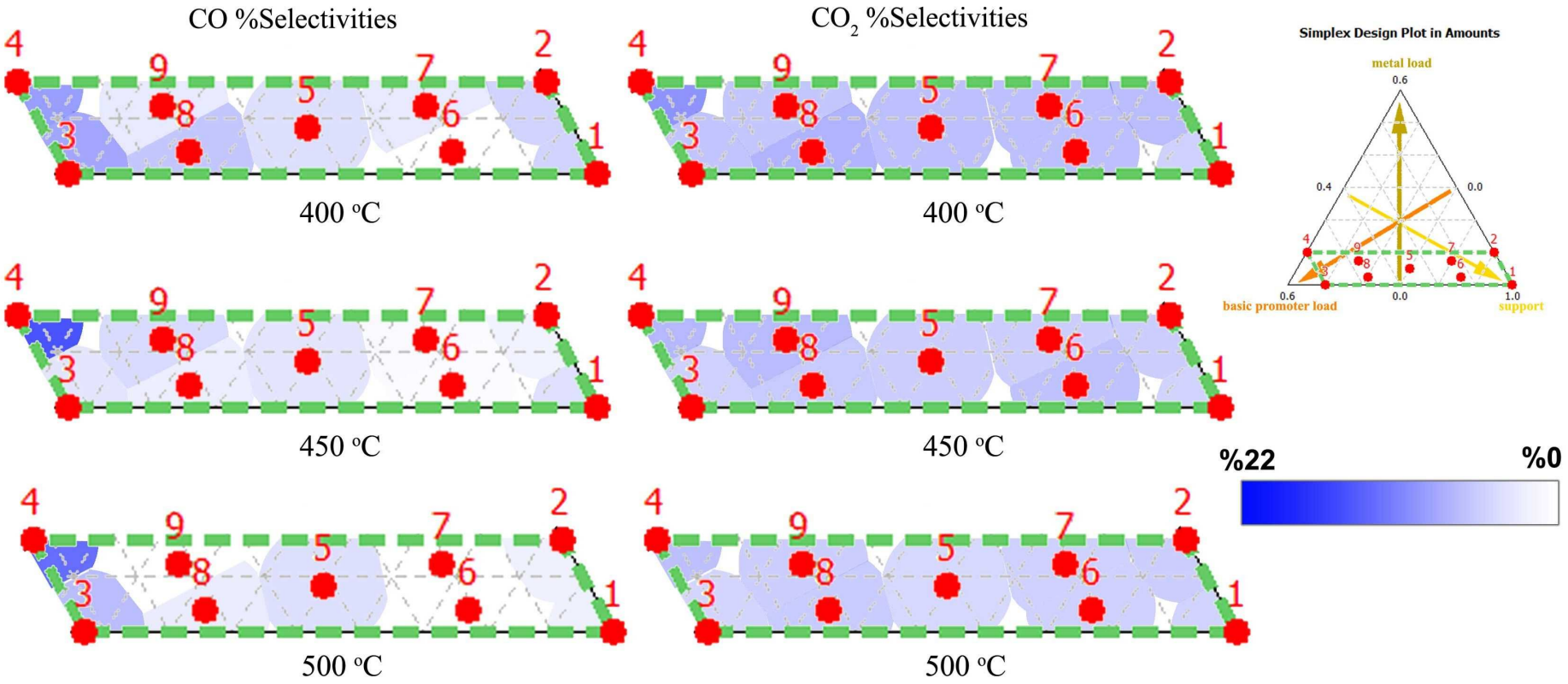

Figure 4.16: Selectivity of CO_2 and CO for different temperatures over total carbon feed for $Fe/MgO/Al_2O_3$ catalysts.

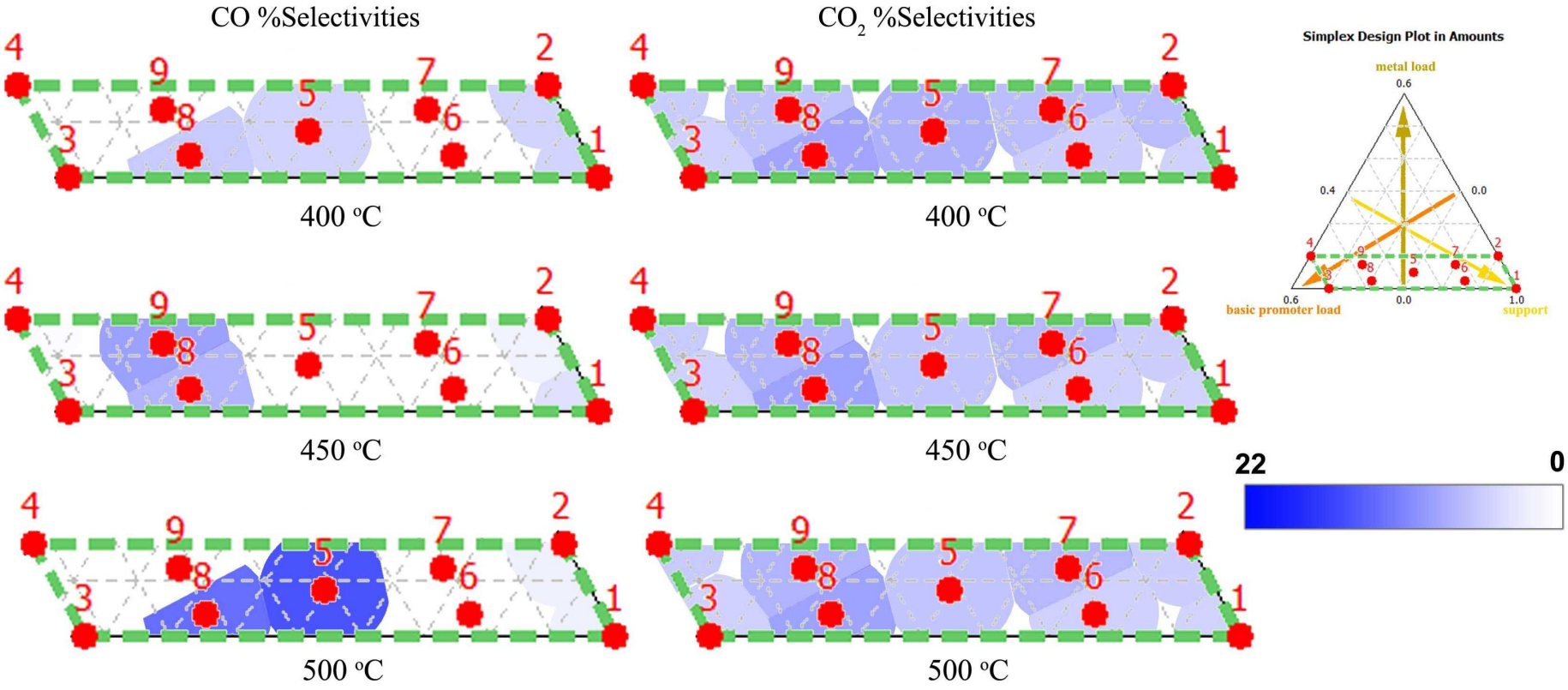

Figure 4.17: Selectivity of CO_2 and CO for different temperatures over total carbon feed for $Fe/CeO_2O/Al_2O_3$ catalysts.

Besides, the basicity effects on the catalyst activity show that crystallite size affects product selectivity. It is observed that increased MgO crystallite size from <5 nm to 34.1 nm for 50% MgO/Al_2O_3 2.5/12.5% $Fe/MgO/Al_2O_3$ results in the gas phase selectivity towards CO. Additionally, the decrease in gas phase selectivity with increased crystallite size of FeO from XRD amorphous sizes to 7.5 nm observed when 10% Fe/Al_2O_3 and 7.5/37.5% $Fe/MgO/Al_2O_3$ were compared. This effect of crystallite size change of iron oxide can explain the low activity of Fe in some studies [Suzuki 2005, Kunkes 2009]. A similar effect of crystallite size was studied for Pt promoted catalysts [Lehnert 2008]. In these studies, the crystallite size effects were not considered. Similarly, the effect of crystallite size of MgO as basic promoter was not considered in any of the studies [Bobadilla 2012, Adhikari 2008, Soares 2006].

Calculated H_2 selectivity and %yield values are given in Table 4.10 and 4.11 and the change of % yield was illustrated in Figures 4.15 and 4.16. Although the gaseous product selectivity of CF4, 50% CeO_2/Al_2O_3, is the lowest, it has a significant $\%H_2$ yield at all the temperatures.

Most of the CeO_2 containing catalysts, CF6 and CF7, as well as MgO containing Catalysts, MF6 and MF7 catalysts, show the same behaviour for selectivity and yield results in zero selectivity to CO and a small selectivity to CO_2. They have different basicity and basic strengths but their basic promoter loadings are low and they all show similar behaviour as compared to 10% Fe/Al_2O_3. Thus, for these catalysts, transition metal sites rather than basic sites are dominant in catalytic activity. CO_2 results from dehydrogenation of the C–OH bond to an aldehyde or ketone (with formation of H_2) followed by C–C bond cleavage of the carbonyl group (Tanabe 1989) as shown as the reaction paths (19) and (20) in Figure 4.13. But the reaction through this path results in low gaseous product selectivity as observed from the catalyst tests.

It is also observed that with increased gaseous product selectivity, $\%H_2$ yield is decreased significantly. WGS tends to move towards formation of CO and H_2O from CO_2 and H_2. Especially, at high temperatures as gaseous products selectivity increases. This behaviour can clearly be observed from the activities of more basic catalysts.

Table 4.12. Selectivity and % Yield of H_2 over total carbon feed for $Fe/MgO/Al_2O_3$ catalysts

	H_2 Selectivity			**% H_2 Yield**		
Catalyst\Temperature (ºC)	400	450	500	400	450	500
Al_2O_3	1.84	1.94	2.08	79	83	89
10% Fe/Al_2O_3	1.96	2.12	2.11	84	91	91
50% MgO/Al_2O_3	1.74	1.99	1.72	75	85	74
10/50% $Fe/MgO/Al_2O_3$	1.85	1.62	1.64	79	69	70
5/25% $Fe/MgO/Al_2O_3$	1.98	2.01	1.90	85	86	82
2.5/12.5% $Fe/MgO/Al_2O_3$	2.30	2.30	2.31	99	99	99
7.5/12.5% $Fe/MgO/Al_2O_3$	2.04	2.26	2.32	87	97	100
2.5/37.5% $Fe/MgO/Al_2O_3$	1.93	2.08	2.06	83	89	88
7.5/37.5% $Fe/MgO/Al_2O_3$	2.10	1.98	2.32	90	85	100

Table 4.13. Selectivity and % Yield of H_2 over total carbon feed for $Fe/CeO_2/Al_2O_3$ catalysts.

	H_2 Selectivity			**% H_2 Yield**		
Catalyst\Temperature (ºC)	400	450	500	400	450	500
Al_2O_3	1.84	1.94	2.08	79	83	89
10% Fe/Al_2O_3	1.96	2.12	2.11	84	91	91
50% CeO/Al_2O_3	2.32	2.32	2.32	100	100	100
10/50% $Fe/CeO/Al_2O_3$	2.30	2.29	2.32	99	98	100
5/25% $Fe/CeO/Al_2O_3$	2.00	2.33	1.59	86	100	68
2.5/12.5% $Fe/CeO/Al_2O_3$	2.33	2.33	2.33	100	100	100
7.5/12.5% $Fe/CeO/Al_2O_3$	2.32	2.33	2.33	100	100	100
2.5/37.5% $Fe/CeO/Al_2O_3$	1.95	1.85	1.72	83	79	74
7.5/37.5% $Fe/CeO/Al_2O_3$	2.32	1.78	2.33	100	76	100

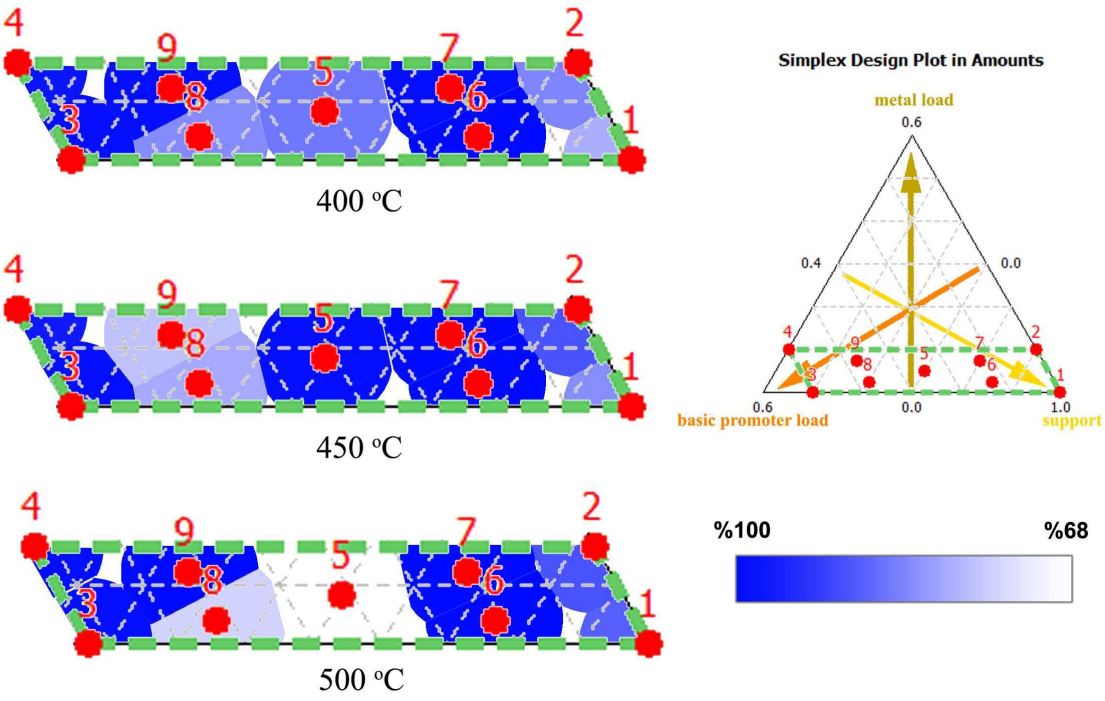

Figure 4.18: % Yield of H_2 over total carbon feed for $Fe/CeO_2/Al_2O_3$ catalysts.

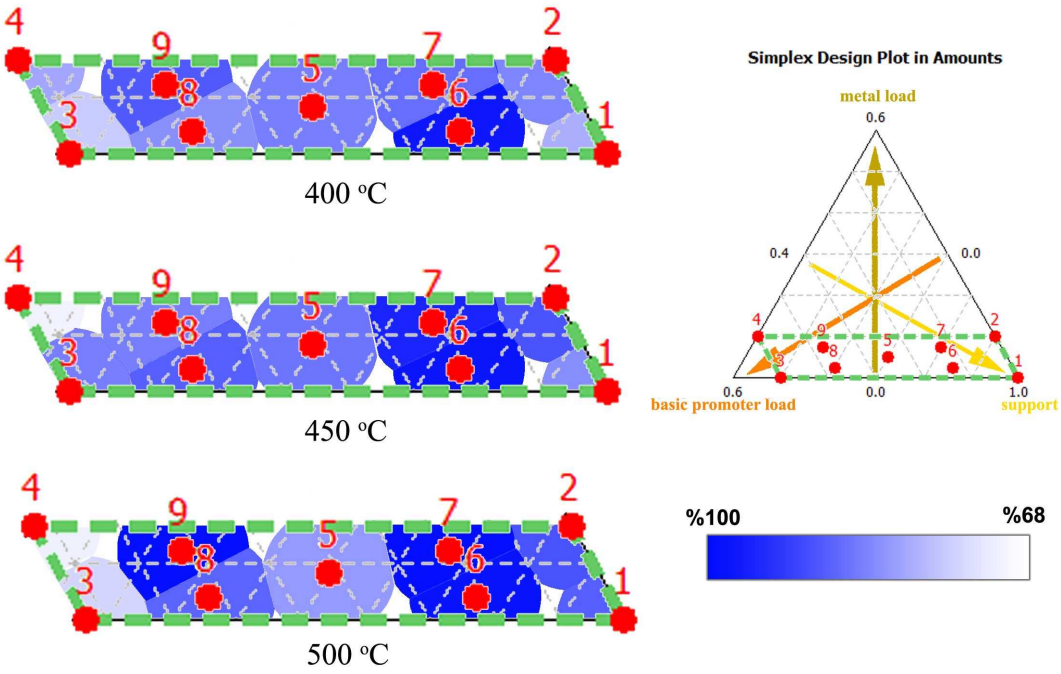

Figure 4.19: % Yield of H_2 over total carbon feed for $Fe/MgO/Al_2O_3$ catalysts.

CHAPTER 5

CONCLUSIONS

In this study, the effect of the basicity and/or basic strength of support material, on activity and hydrogen selectivity in the steam reforming of glycerol over transition metal, iron, supported on magnesium oxide (MgO) and cerium oxide (CeO_2) modified alumina (Al_2O_3) catalysts was investigated. Catalyst activity tests show that glycerol decomposes to liquid phase products and conversion increased with increased temperature from 400 to 500 ºC. But the presence of a catalyst was required for gas phase products at both low and high temperatures. Catalysts also promote the conversion of glycerol at low temperatures for all the catalysts.

It is observed that the presence of Fe for MgO supported catalysts; gas product selectivity increases unless FeO crystallite size becomes higher than ~5 nm. And it is also observed that larger MgO crystallites size shifts gaseous product selectivity towards CO. No CH_4 was observed in the gas phase on all the catalysts which indicates that the prepared catalysts have high water gas shift (WGS) activities. A similar behaviour observed for catalysts with higher basicity and the presence of unidantete carbonate basic sites observed at 865 and 800 cm^{-1} FTIR bands for CeO_2 promoted catalysts. Also, CO formation was hindered and CO_2 formation was favoured on CeO_2 promoted catalysts with unidentate carbonate basic sites. This also results in high activity of steam reforming. Furthermore, CeO_2 promoted catalysts results in only trace amounts of EtOH and MeOH in liquid phase products as compared to MgO supported catalysts. The additions of Fe to CeO_2 supported catalysts do not change glycerol conversion and the gaseous product selectivity significantly. Basicity measurements show that inorganic carboxylate site having FTIR band of 1535 and 1410 cm^{-1} is dominantly effective for gaseous product selectivity. High total basicity does not give for high glycerol conversion, yet high total basicity results in high gaseous product selectivity. Also, at low total basicity, gaseous product selectivity decreased with increased temperature. It is also observed that with increased gaseous product selectivity, H_2 yield is decreased significantly. WGS tends to move towards formation of CO and H_2O from CO_2 and H_2; especially at high temperatures as gaseous products

selectivity increases. This behaviour can be clearly observed from the activities of more basic catalysts.

Considering studied catalysts, it can be concluded that MgO and FeO modified catalysts shows better activity for syn-gas production due to their basic and crystalline properties. And CeO_2 modified catalysts and MgO catalysts with crystallite sizes lower than 5 nm are shows better performances for CO free product.

APPENDIX

APPENDIX A

XRD spectra of catalysts

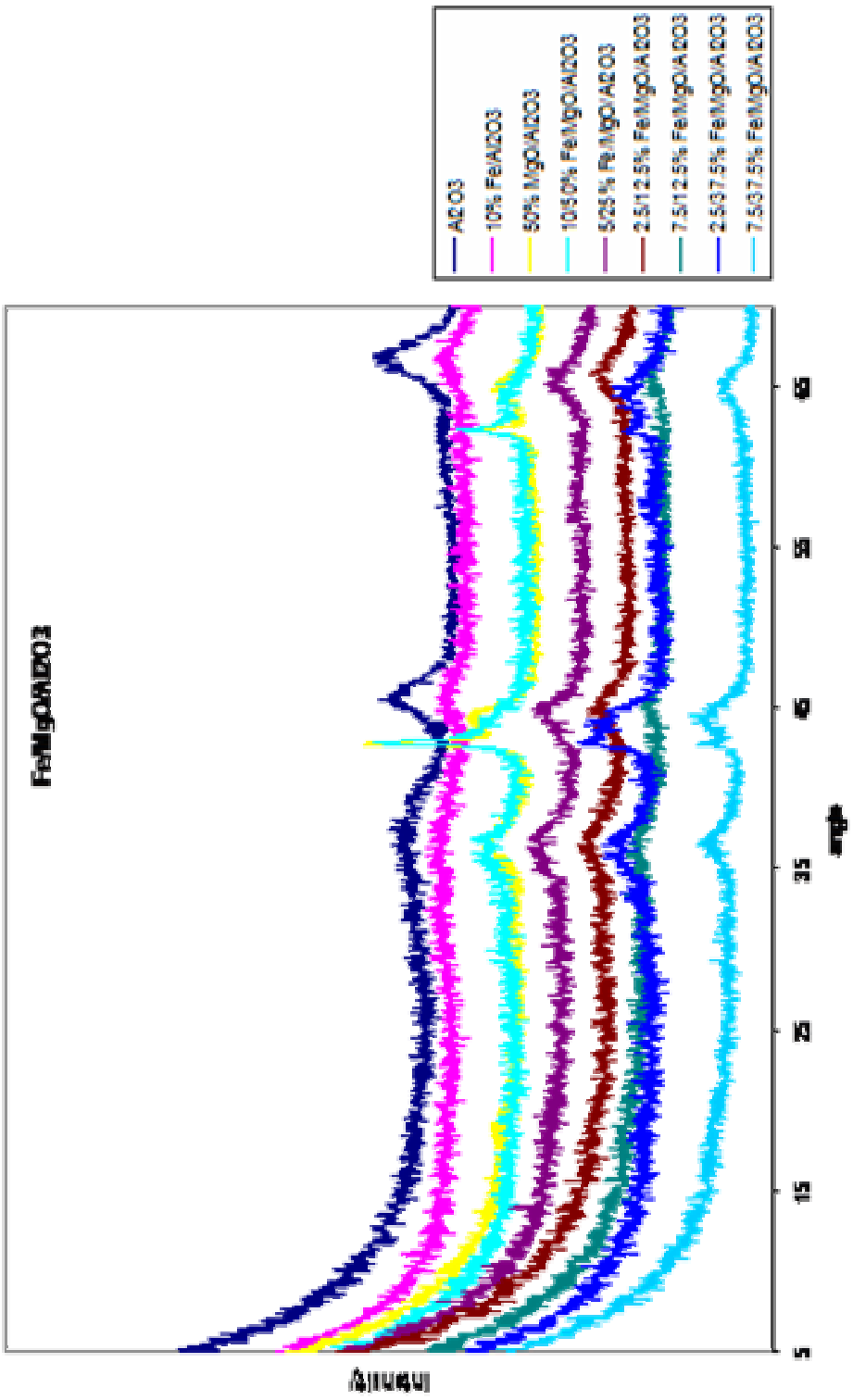

Figure A.1. Comparison of XRD results for Fe on MgO/Al_2O_3 catalysts.

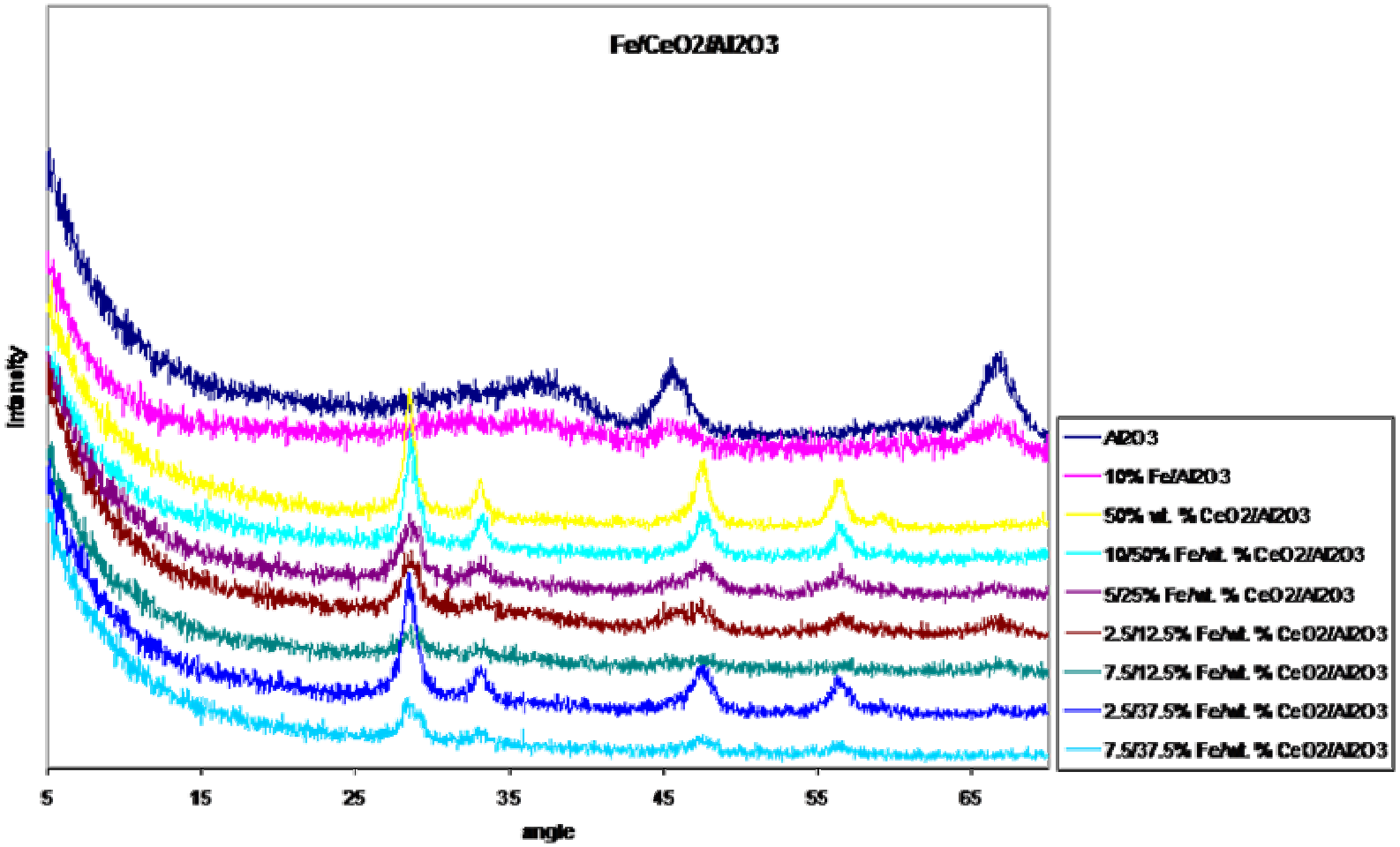

Figure A.2. Comparison of XRD results for Fe on CeO_2/Al_2O_3 catalysts

APPENDIX B
FTIR spectra of catalysts

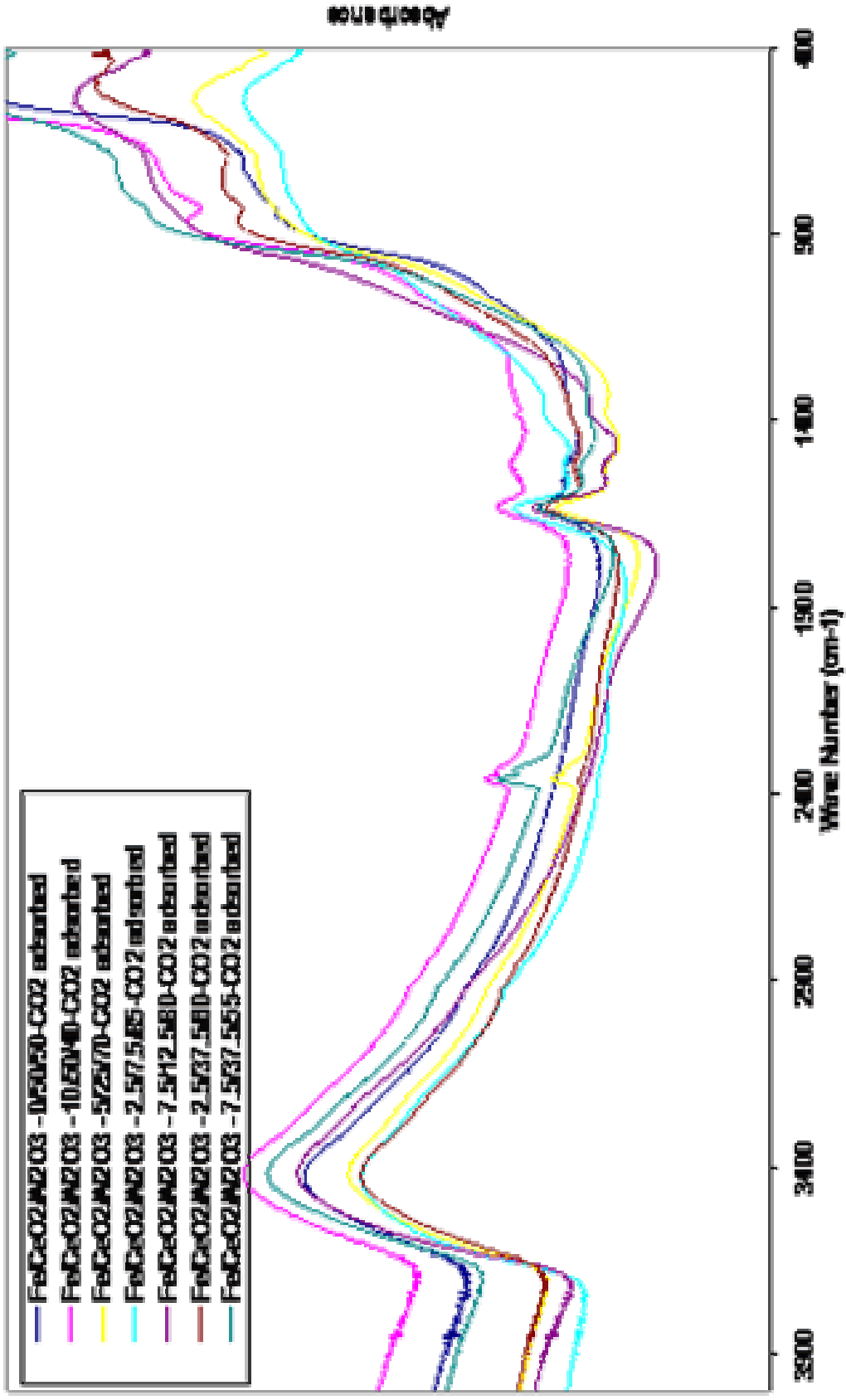

Figure B.1. FTIR spectra of CO_2 adsorbed Fe on CeO_2/Al_2O_3 catalysts

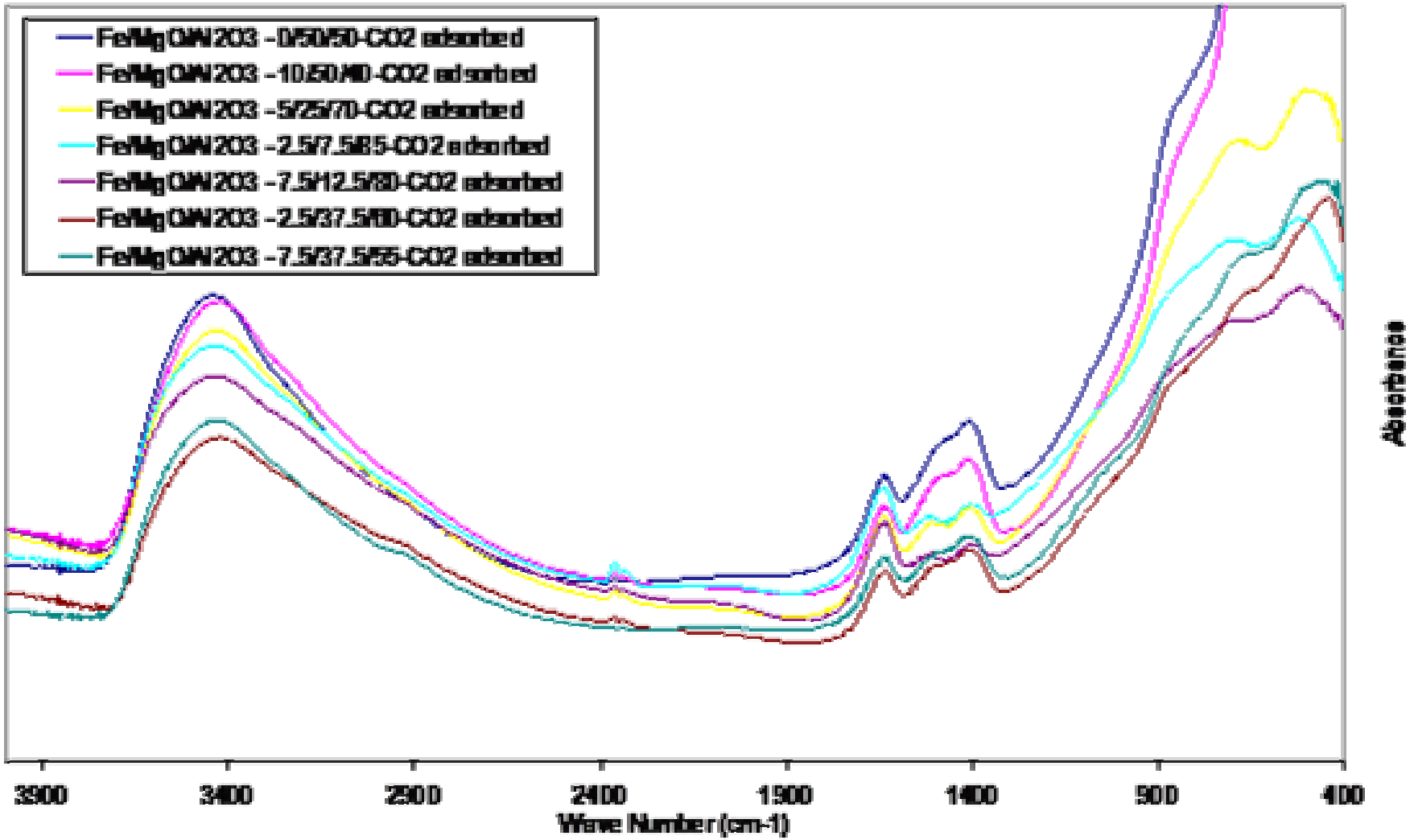

Figure B.2.: FTIR spectra of CO_2 adsorbed Fe on MgO/Al_2O_3 catalysts

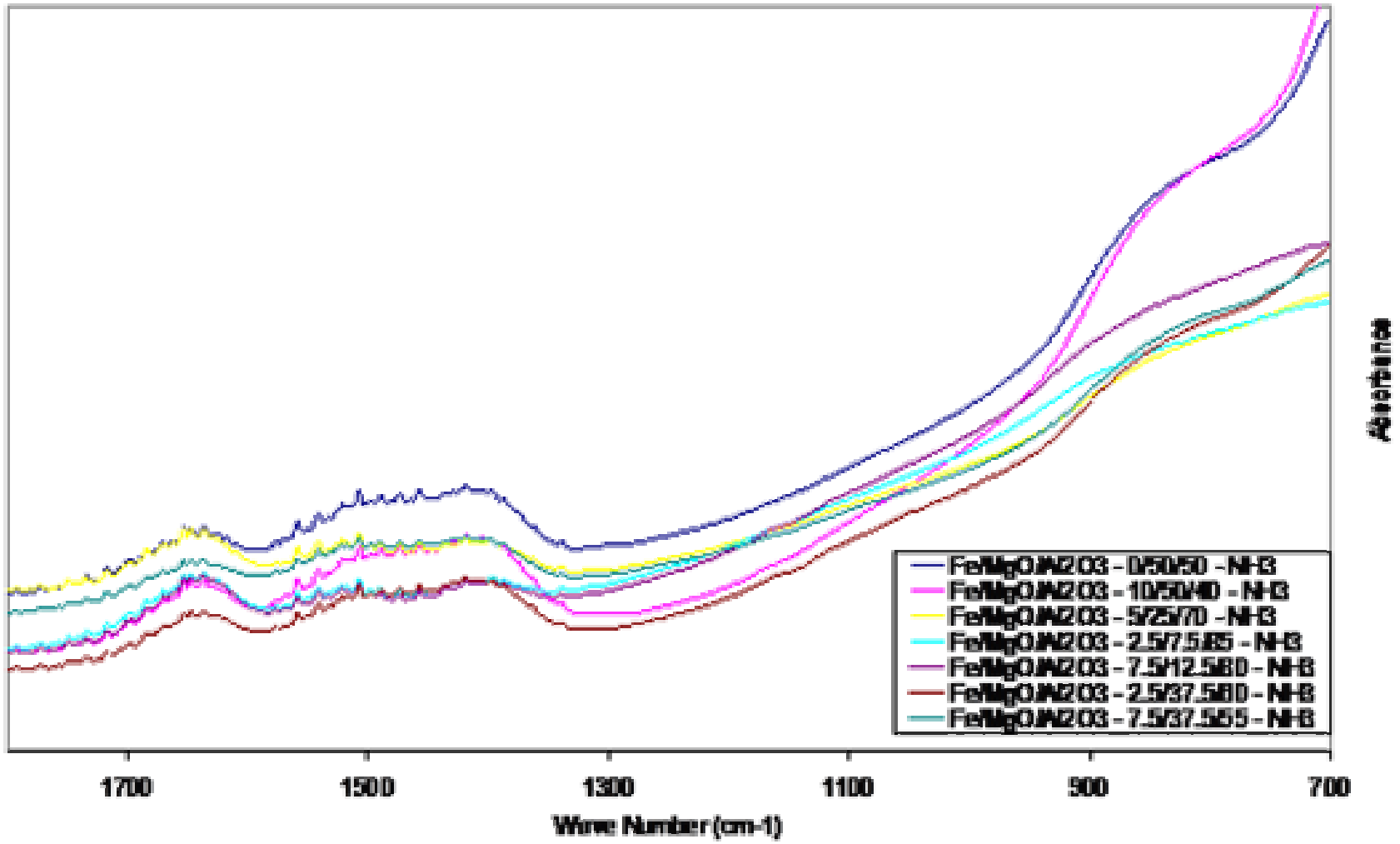

Figure B.3.: FTIR spectra of HNO_3 adsorbed Fe on MgO/Al_2O_3 catalysts

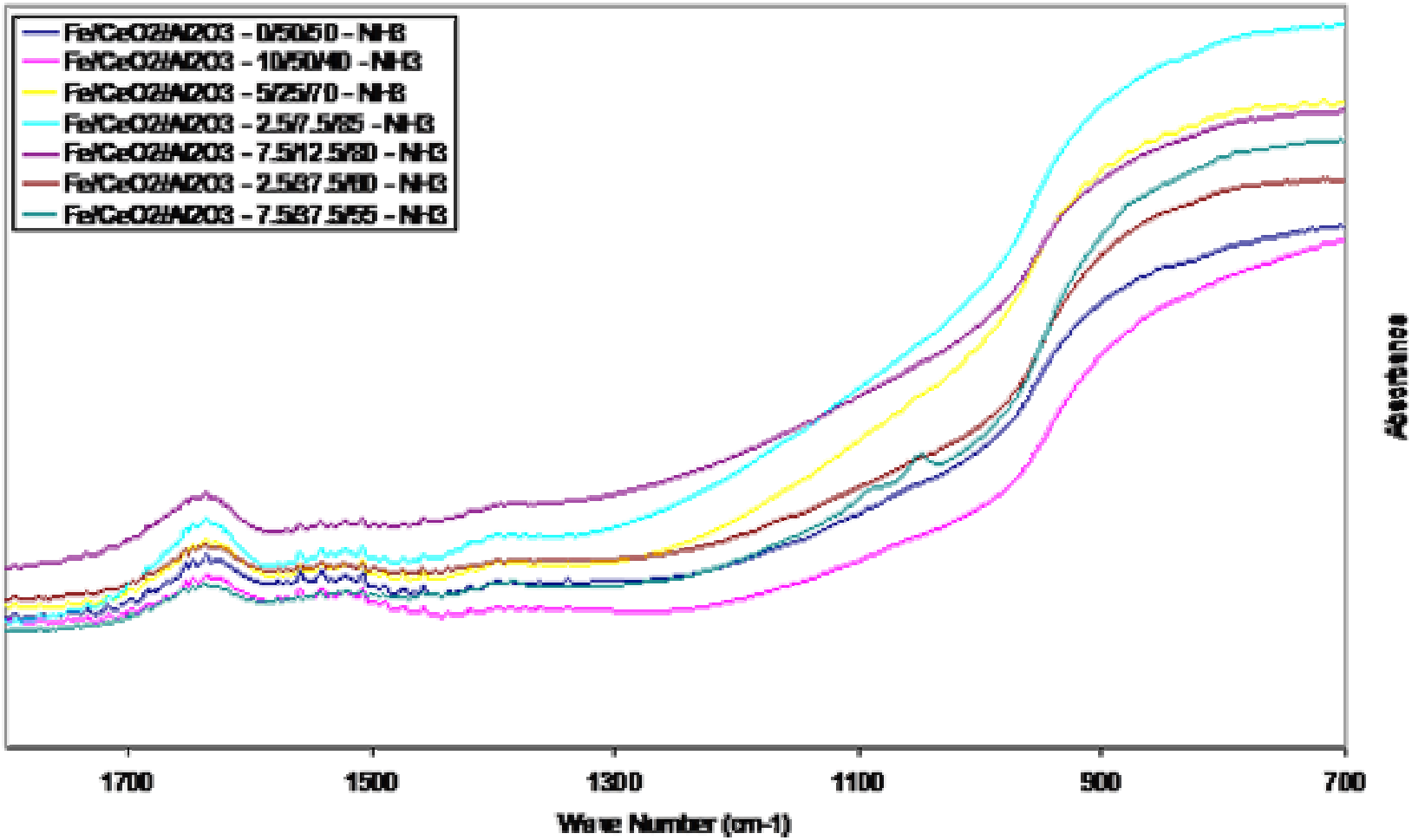

Figure B.4.: FTIR spectra of HNO_3 adsorbed Fe on CeO_2/Al_2O_3 catalysts

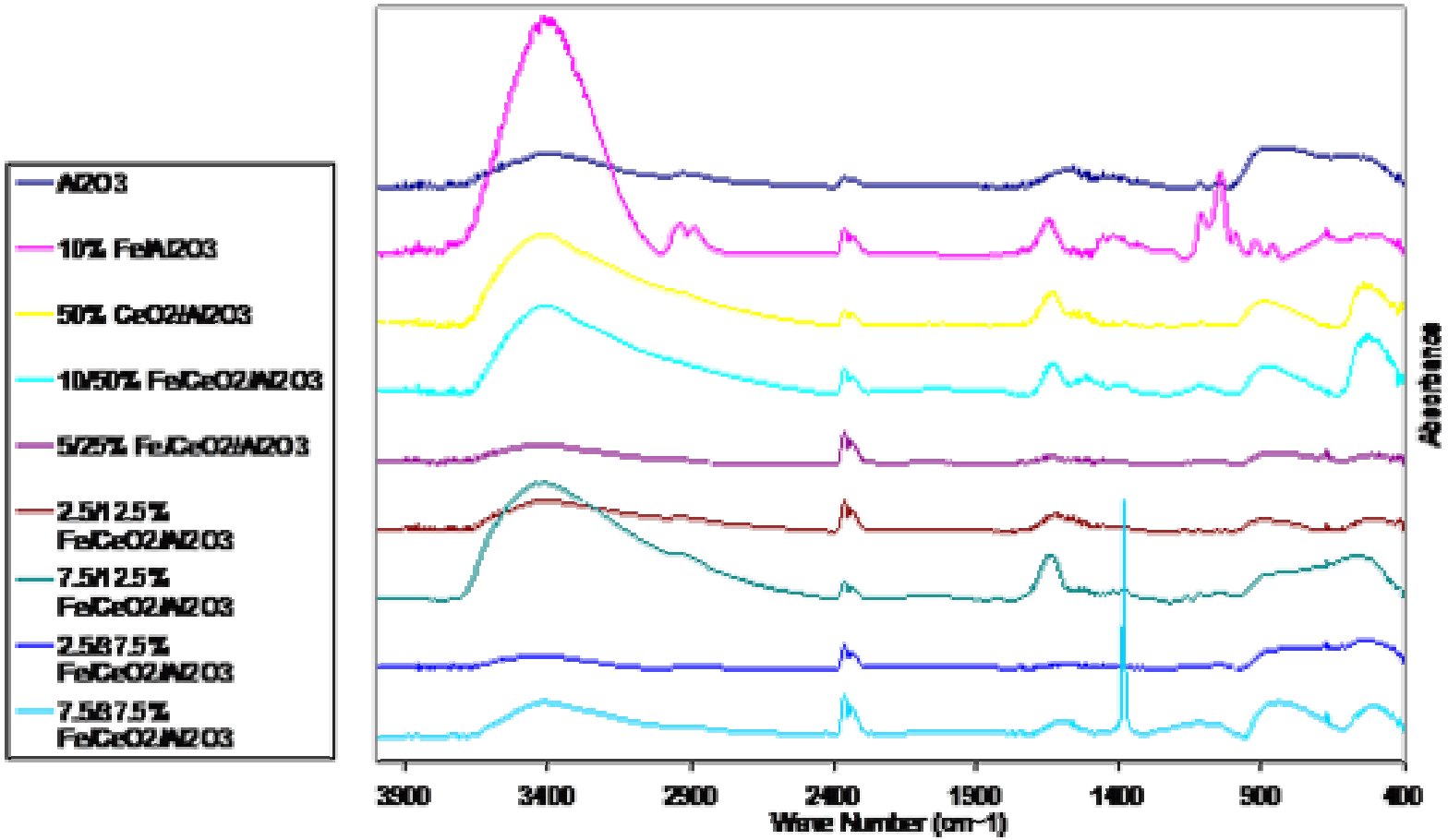

Figure B.5.: FTIR spectra of used Fe on MgO/Al_2O_3 catalysts

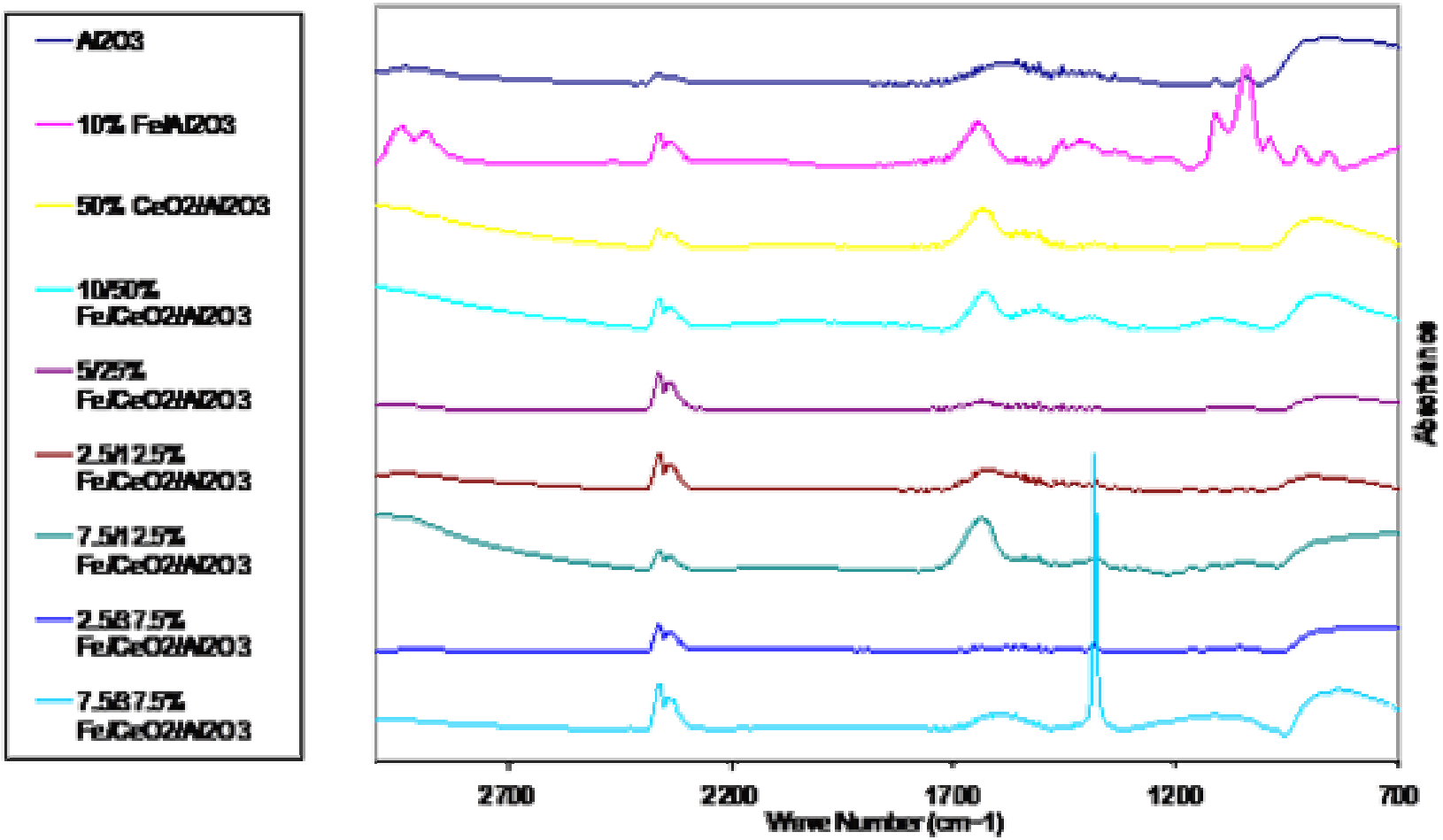

Figure B.6.. FTIR spectra of used Fe on CeO_2/Al_2O_3 catalysts FTIR.

APPENDIX C
Representative Gas phase gas chromatograph

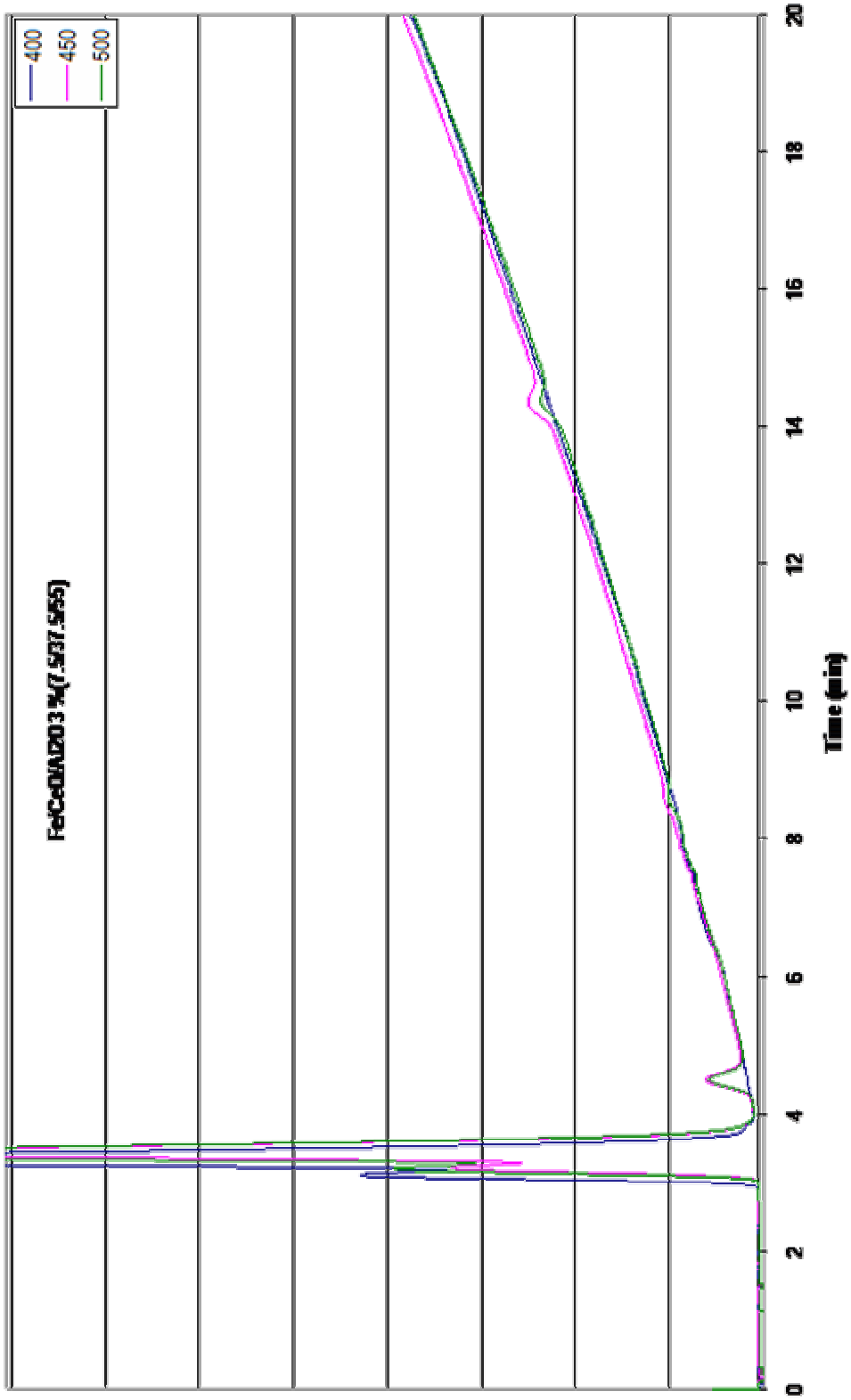

Figure C.1: Gas chromatograph of catalyst testing of $Fe/CeO_2/Al_2O_3$ with loadings % 7.5, % 37.5 and % 55 respectively.

APPENDIX D

Liquid phase FTIR analyze validation

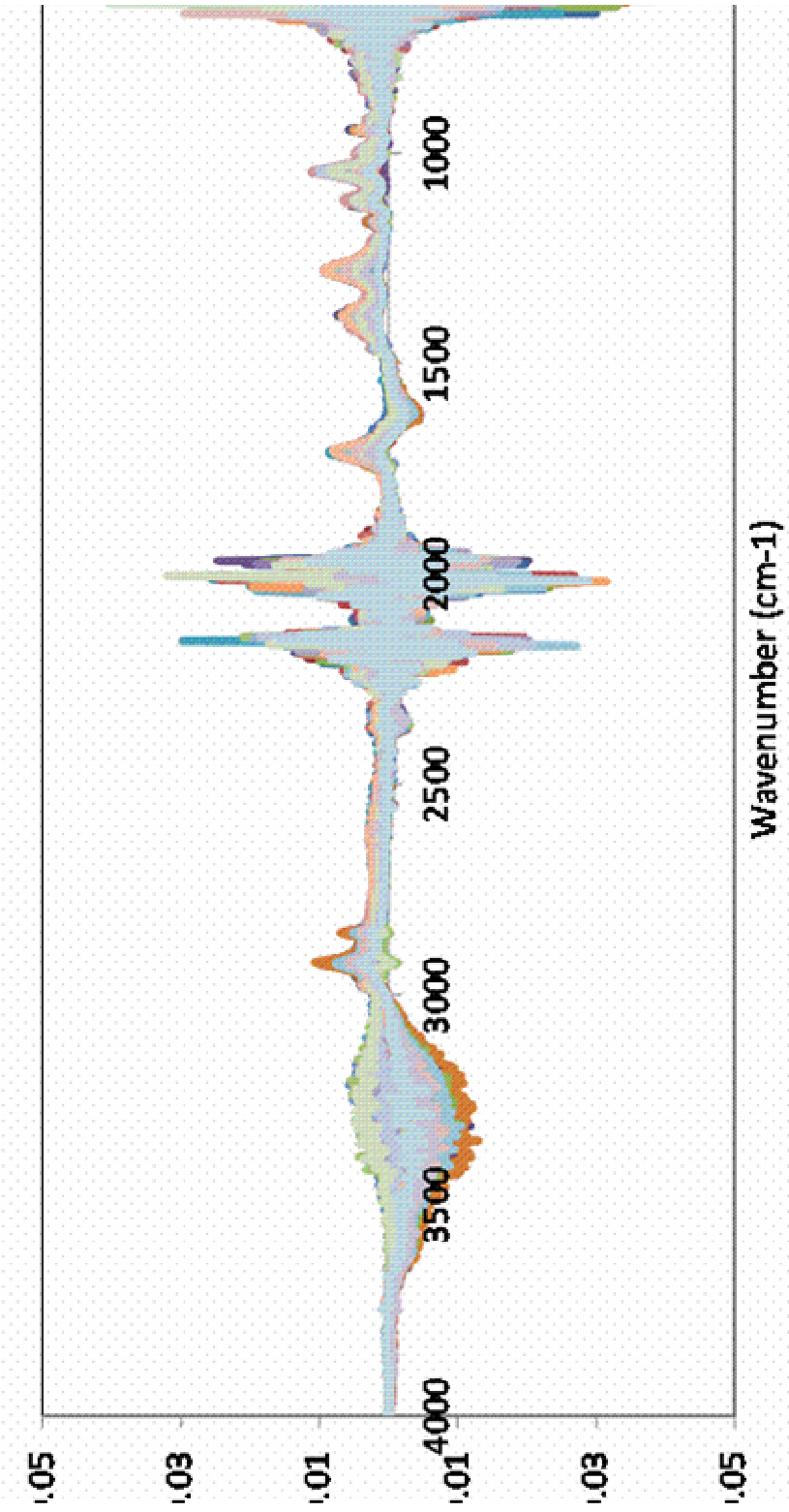

Figure D.1: FTIR spectra of quaternary mixtures of water, glycerol, isopropyl alcohol and acetic acid (pure water is taken as background).

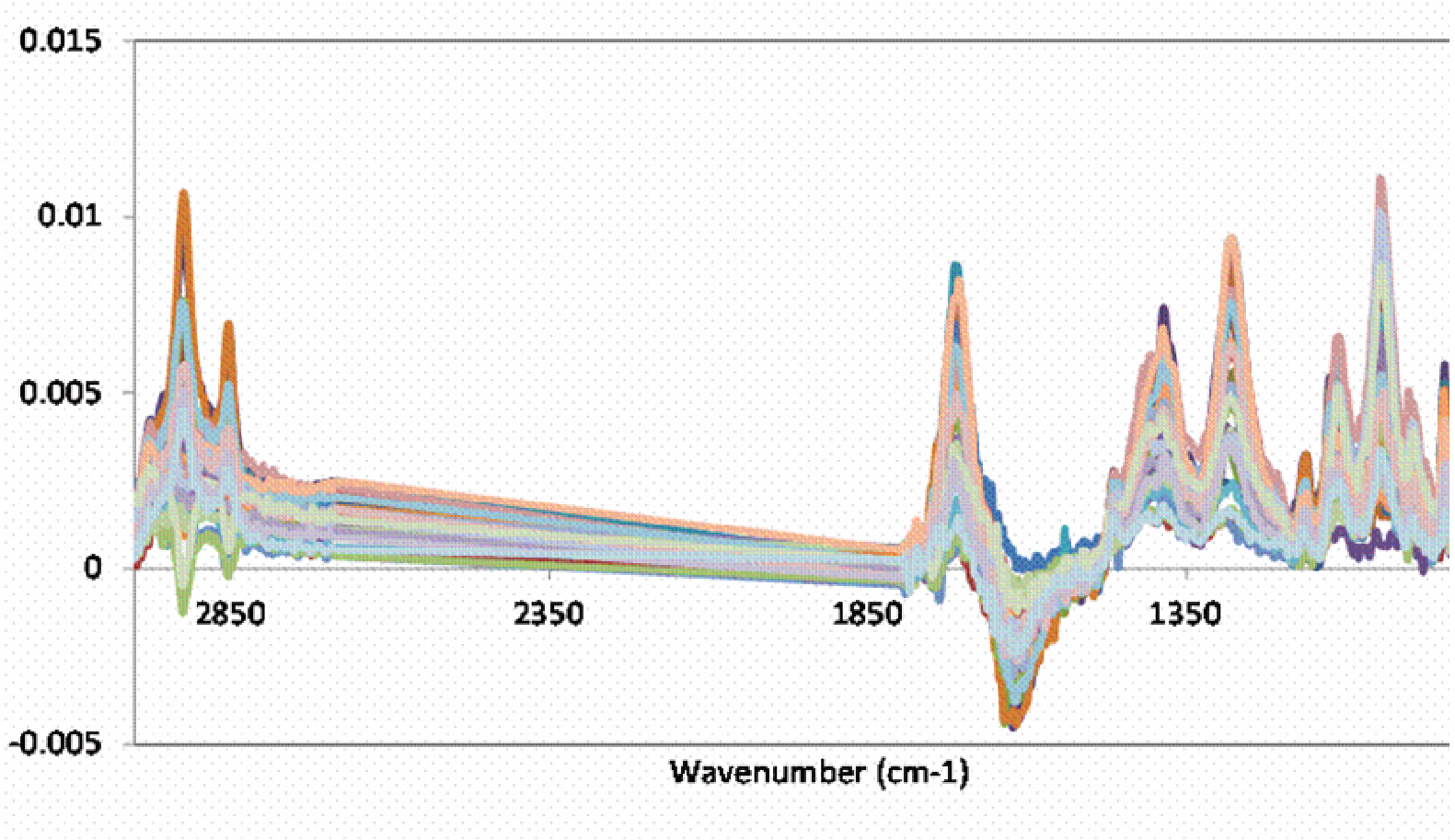

Figure D.2: FTIR spectra of quaternary mixtures of water, glycerol, isopropyl alcohol and acetic acid (pure water is taken as background and noise regions are removed).

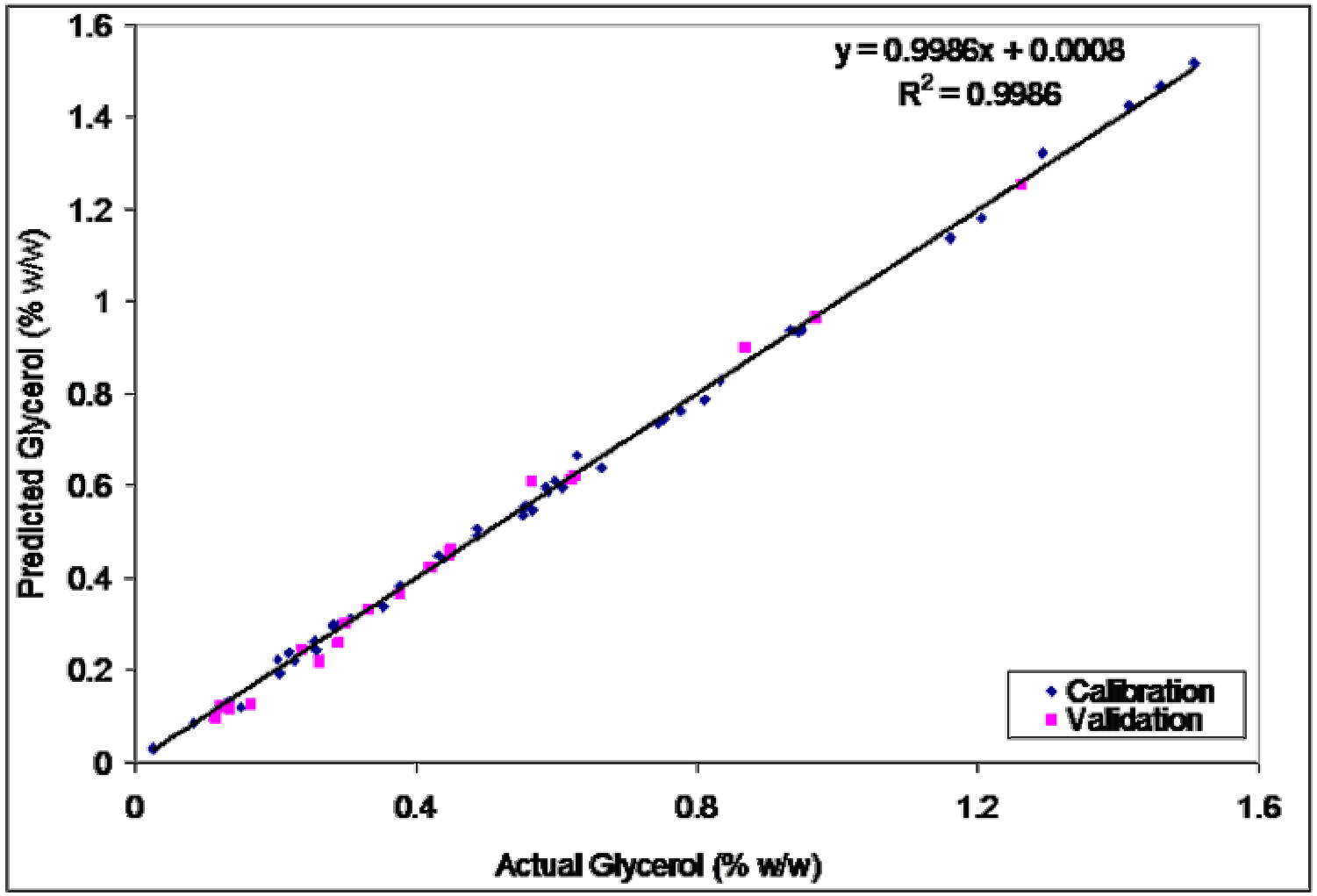

Figure D.3: Reference versus FTIR-predicted glycerol content of validation samples.

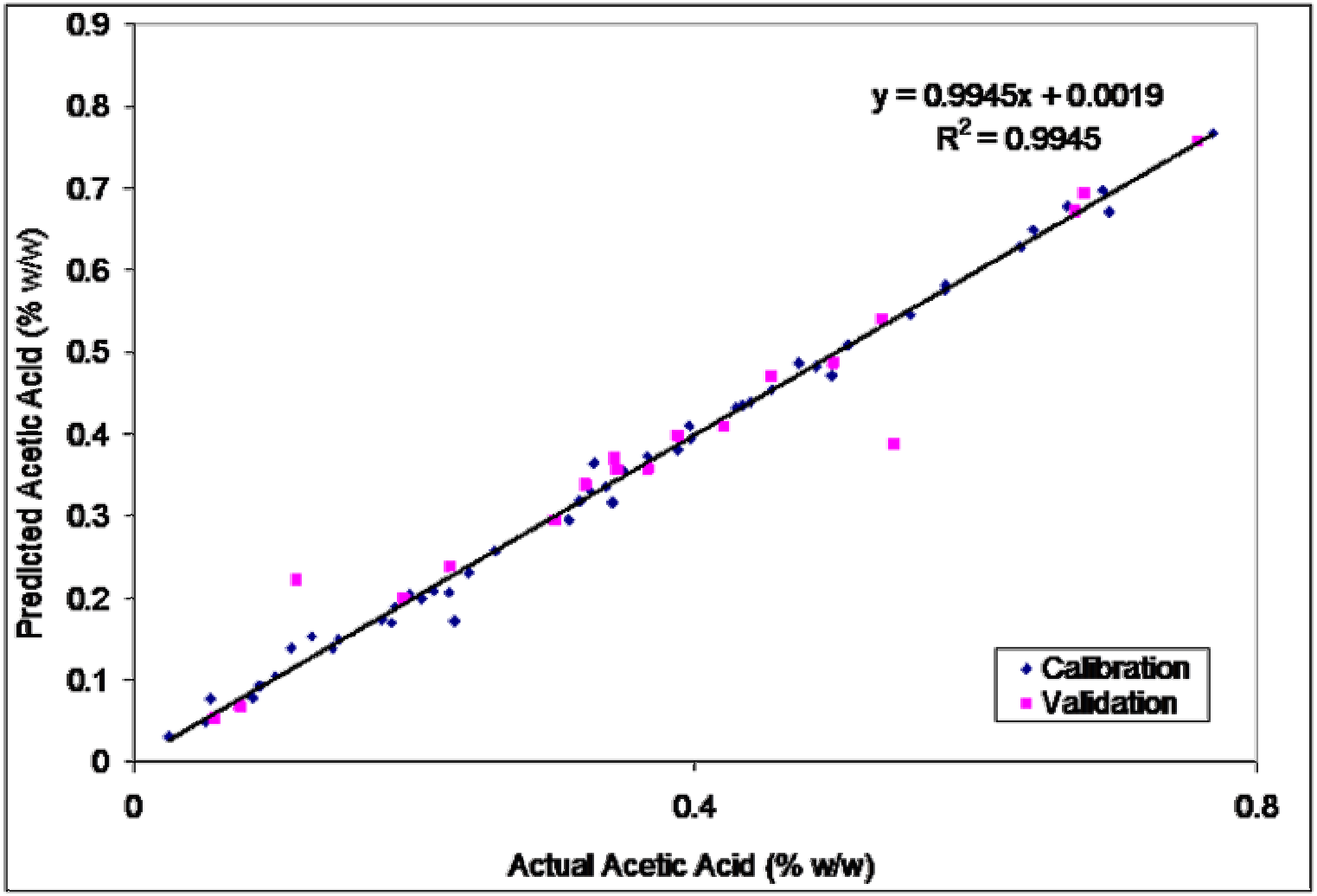

Figure D.4: Reference versus FTIR-predicted acetic acid content of validation samples.

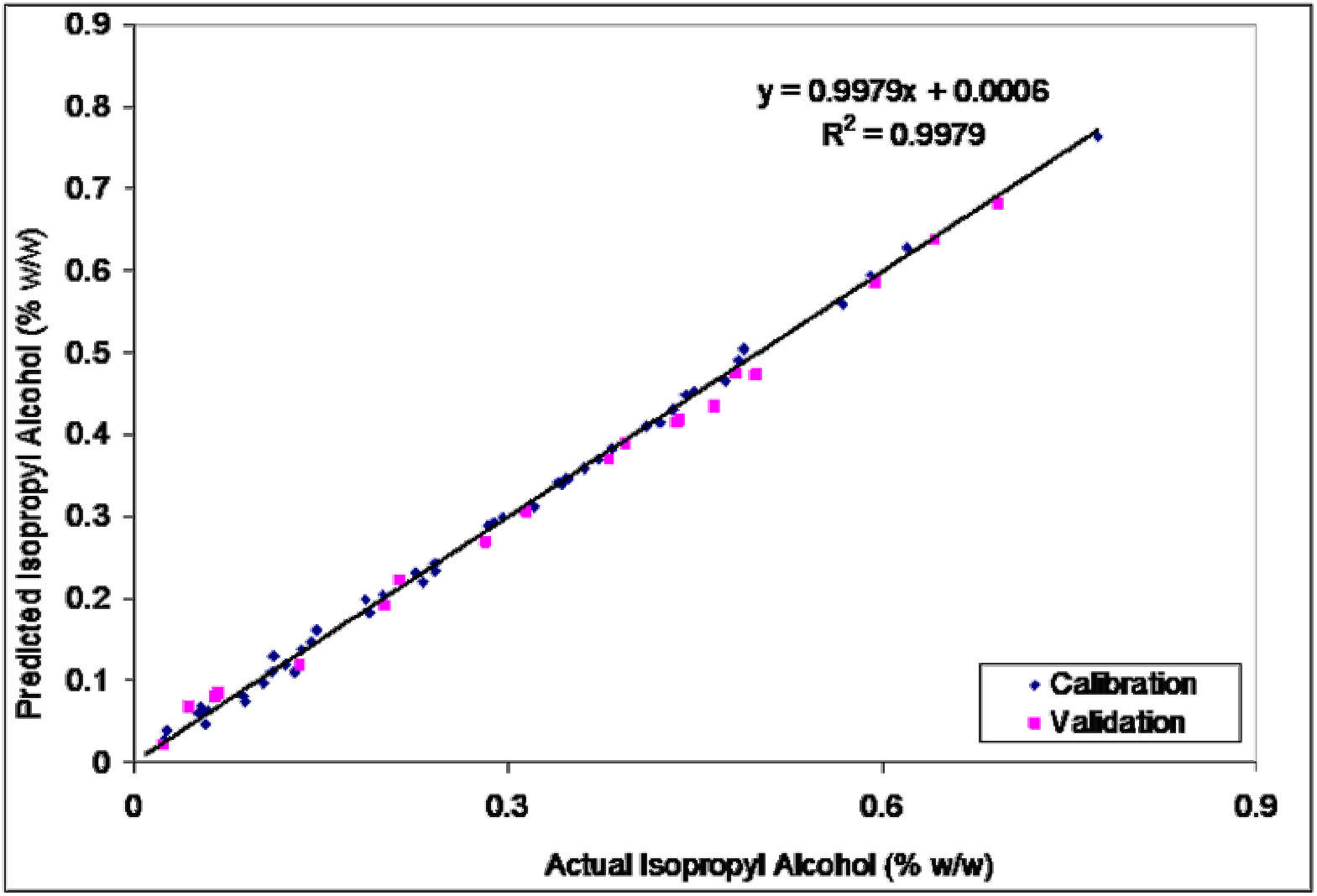

Figure D.5: Reference versus FTIR-predicted isopropyl alcohol content of validation samples.

REFERENCES

Adesina A., Chin Kui Cheng, Say Yei Foo, Adesoji A., "Glycerol Steam Reforming over Bimetallic Co-Ni/Al_2O_3", Ind. Eng. Chem. Res., 49, 10804–10817, 2010

Fernando S. D., Agus Haryanto, Adhikari Sushil, "Hydrogen production from glycerol: An update", Energy Conversion and Management, 50, 2600–2604, 2009

Adhikari S., Sandun D. Fernando, Agus Haryanto, "Hydrogen production from glycerin by steam reforming over nickel catalysts", Renewable Energy, 33, 1097–1100, 2008

Adhikari S., Sandun D. Fernando, S. D. Filip To, R. Mark Bricka, Philip H. Steele, Agus Haryanto, "Conversion of Glycerol to Hydrogen via a Steam Reforming Process over Nickel Catalysts", Energy & Fuels, 22, 1220–1226, 2008

Bobadilla L.F., A. Álvarez, M.I. Domínguez, F. Romero-Sarria, M.A. Centeno, M. Montes, J.A. Odriozola, "Influence of the shape of Ni catalysts in the glycerol steam reforming", Applied Catalysis B: Environmental 123– 124, 379– 390, 2012

Brown Michael E., Patrick Kent Gallagher, "Handbook of Thermal Analysis and Calorimetry: Recent Advances, Techniques and Applications", Elsevier Science; 1st edition, pg. 388, 2007

Chen De, Li He, Jacobo Manuel Salamanca Parra, Edd Anders Blekkan, "Towards efficient hydrogen production from glycerol by sorption enhanced steam reforming", Energy Environ. Sci., 3, 1046–1056, 2010

Chiodo V., S. Freni, A. Galvagno, N. Mondello, F. Frusteri, "Catalytic features of Rh and Ni supported catalysts in the steam reforming of glycerol to produce hydrogen", Applied Catalysis A: General, 381, 1–7, 2010

Lehnert K., Peter Claus, "Influence of Pt particle size and support type on the aqueous-phase reforming of glycerol", Catalysis Communications, 9, 2543–2546, 2008

Coates John, "Interpretation of Infrared Spectra, A Practical Approach", Encyclopedia of Analytical Chemistry R.A. Meyers (Ed.) pp. 10815–10837, John Wiley & Sons Ltd, Chichester, 2000

Comelli Raul A., Esteban A. Sanchez, Miguel A. D. Angelo “Hydrogen production from glycerol on Ni/Al_2O_3 catalyst”, International journal of hydrogen energy, 35, 5902 – 5907, 2010

Valliyappan T., A. K.Dalai, N.N. Bakhshi, “Pyrolysis of glycerol for the production of hydrogen or syn gas”, Bioresource Technology, 99, 4476–4483, 2008

Ding Y., Haisheng Chen, Tianfu Zhang, Bilin Dou, Valerie Dupont, Paul Williams, Mojtaba Ghadiri, “Thermodynamic analyses of adsorption-enhanced steam reforming of glycerol for hydrogen production”, International journal of hydrogen energy, 34, 7208 – 7222, 2009

Shabaker J. W., Dumesic J. A., G. W. Huber, “Aqueous-phase reforming of oxygenated hydrocarbons over Sn-modified Ni catalysts”, Journal of Catalysis, 222, 180–191, 2004

Cortright R. D., Dumesic J. A., R. R. Davda, “Hydrogen from catalytic reforming of biomass-derived hydrocarbons in liquid water”, Nature, Vol 418, 964 – 967, 2002

Soares R. R., Dumesic J. A., Dante A. Simonetti, “Glycerol as a Source for Fuels and Chemicals by Low-Temperature Catalytic Processing” Angew. Chem. Int. Ed., 45, 3982 –3985, 2006

Kunkes E. L., J. A. Dumesic, Ricardo R. Soares, Dante A. Simonetti, “An integrated catalytic approach for the production of hydrogen by glycerol reforming coupled with water-gas shift”, Applied Catalysis B: Environmental, article in press, 2009

Dietrich P. J., James A. Dumesic, Rodrigo J. Lobo-Lapidus, Tianpin Wu, Aslihan Sumer, M. Cem Akatay, Bradley R. Fingland, Neng Guo, Christopher L. Marshall, Eric Stach, Julius Jellinek, W. Nicholas Delgass, Fabio H. Ribeiro, Jeffrey T. Miller, “Aqueous Phase Glycerol Reforming by PtMo Bimetallic Nano-Particle Catalyst: Product Selectivity and Structural Characterization”, Top Catal, 55:53–69, 2012

Ertl G., H. Knozinger, F. Shüth, J. Weitkamp, “Handbook of Heterogeneous Catalysis”, Wiley, 3018 – 3050, 2008.

Adhikari S., Sandun D. Fernando, Agus Haryanto" Hydrogen production from glycerin by steam reforming over nickel catalysts", Renewable Energy, 33, 1097–1100, 2008

Adhikari S., Sandun Fernando, Steven R. Gwaltney, S.D. Filip To, R. Mark Brick, Philip H. Steele, Agus Haryanto, "A thermodynamic analysis of hydrogen production by steam reforming of glycerol", International Journal of Hydrogen Energy, 32, 2875 – 2880, 2008

Iriondo A., J.F. Cambra, V.L. Barrio, M.B. Guemez, P.L. Arias, M.C. Sanchez-Sanchez, R.M. Navarro, J.L.G. Fierro, "Glycerol liquid phase conversion over monometallic and bimetallic catalysts: Effect of metal, support type and reaction temperatures", Applied Catalysis B: Environmental, 106, 83– 93, 2011

T. Jin, Y. Zhou, G. J. Mains, J. M. White, "Infrared and X-ray Photoelectron Spectroscopy Study of CO and CO, on Pt/CeO_2" J. Phys. Chem., 91, 5931 – 5937, 1987

Ma Xinbin, Hao Wang, Xiaodong Wang, Maoshuai Li, Shuirong Li, Shengping Wang, "Thermodynamic analysis of hydrogen production from glycerol autothermal reforming", International journal of hydrogen energy, 34, 5683 – 5690, 2009

Maulijin J. A., P. W. N. M. Van Leeuwen, R. A. Van Santen, "Catalysis an integrated approach to Homogeneous, Heterogeneous and Industrial Catalysis", Elsevier, 90 – 95, 1993

Mousdale David M., "Biofuels Biotechnology, Chemistry, and Sustainable Development", CRC Press, 2008

Nichele Valentina, Michela Signoretto, Federica Menegazzo, Alessandro Gallo, Vladimiro Dal Santo, Giusepp Cruciani, Giuseppina Cerrato, "Glycerol steam reforming for hydrogen production: Design of Ni supported catalysts", Applied Catalysis B: Environmental 111– 112, 225– 232, 2012

Buffoni I. N., Francisco Pompeo, Gerardo F. Santori, Nora N. Nichio, "Nickel catalysts applied in steam reforming of glycerol for hydrogen production", Catalysis Communications, article in press, 2009

Pompeo F., Gerardo Santori, Nora N. Nichio, "Hydrogen and/or syngas from steam reforming of glycerol, Study of platinum catalysts", International journal of hydrogen energy, 35, 8912 – 8920, 2010

Pompeo F., Gerardo F. Santori, Nora N. Nichio, “Hydrogen production by glycerol steam reforming with Pt/SiO2 and Ni/SiO2 catalysts” Catalysis Today 172, 183–188, 2011

Neimantsverdriet J. W., “Spectroscopy in Catalysis”, 3rd ed. Wiley VHC, 2007

Li C., Yoshihisa Sakata, Toru Arai, Kazunari Domen, Ken-ichi Maruya, Onishi T., “Carbon Monoxide and Carbon Dioxide Adsorption on Cerium Oxide studied by Fourier- transform Infrared Spectroscopy”, J. Chem. Soc., Faraday Trans. I, 85, 4 929-943, 1989

Özdemir D., B. Üner, İ. Karaman, H. Tanrıverdi, “Determination of lignin and extractive content of Turkish Pine (Pinus brutia Ten.) trees using near infrared spectroscopy and multivariate calibration”, Wood Sci Technol, 45:121–134, 2011

Patil H. M., D. K. Sawant, D.S. Bhavsar, J. H. Patil, K.D. Girase, “Crystallographic and FT-IR Characteristics of Gel Grown Cerium Tartrate Crystals”, Archives of Physics Research, 2 (1): 239 – 245, 2011

Patterson, A. L. 1939. The Scherrer Formula for X-ray Particle Size Determination. Physical Review 56 : 978 – 982.

Santen Rutger A. Van, “Complementary Structure Sensitive and Insensitive Catalytic Relationships”, Accounts Of Chemical Research, Vol. 42, No. 1, 57-66, 2008

Santos M. L. Dos, R.C. Lima, C.S. Riccardi, R.L. Tranquilin, P.R. Bueno, J.A. Varela, E. Longo, "Preparation and characterization of ceria nanospheres by microwave-hydrothermal method", X Materials Letters, 62, 4509 – 4511, 2008

Dauenhauer P.J., L.D. Schmidt, J.R. Salge, “Renewable hydrogen by autothermal steam reforming of volatile carbohydrates”, Journal of Catalysis, 244, 238–247, 2006

Saikia Bhaskar J., Gopalakrishnarao Parthasarathy, "Fourier Transform Infrared Spectroscopic Characterization of Kaolinite from Assam and Meghalaya, Northeastern India", J. Mod. Phys., 1, 206 – 210, 2010

Schmal M, Lucia G. Appel, Jean G. Eon, “The CO2–CeO2 interaction and its role in the CeO2 reactivity”, Catalysis Letters, 56, 199–202, 1998

Nichele Valentina, Michel Signoretto, Federica Menegazzo, Alessandro Gallo, Vladimiro Dal Santo, Giuseppe Cruciani, Giuseppina Cerrato, “Glycerol steam reforming for hydrogen production: Design of Ni supported catalysts”, Applied Catalysis B: Environmental 111– 112, 225– 232, 2012

Singhabhandhu A., Tetsuo Tezuka, “A perspective on incorporation of glycerin purification process in biodiesel plants using waste cooking oil as feedstock”, Energy 35, 2493 – 2504, 2010

Somorjai Gabor A., “Introduction to surface science and catalysis”, Wiley, New York, 1994

Sutar P. N., P. D. Vaidya, A. E. Rodrigues, “Glycerol-Reforming Kinetics Using a Pt/C Catalyst” Chem. Eng. Technol., 33, No. 10, 1645–1649, 2010

Turner J., George Sverdrup, Margaret K. Mann, Pin-Ching Maness, Ben Kroposki, Maria Ghirardi, Robert J. Evans, Dan Blake, “Renewable hydrogen production”, Int. J. Energy Res., 32, 379 – 407, 2008

Swanson Meghan Elizabeth, “Interaction of carbon monoxide with partially reduced ceria-zirconia supported catalysts”, Doctoral Thesis / Dissertation, University of Pittsburgh, 2008

Tanabe K., M. Misono, Y. Ono, H. Hattori, “New Solid Acids and Bases”, Tokyo, Elsevier, 1989

Guodong Wen, Yunpeng Xu, Huaijun Maa, Zhusheng Xu, Tian Zhijian “Production of hydrogen by aqueous-phase reforming of glycerol”, international journal of hydrogen energy, 33, 6657 – 6666, 2008

Umdu E. Selahattin, “Methyl Ester Production from Vegetable Oils On Heteregeneous Basic Catalysts”, 2008

Umdu Emin Selahattin Şeker Erol, Mert Tuncer, “Transesterification of Nannochloropsis oculata microalga’s lipid to biodiesel on Al2O3 supported CaO and MgO catalysts”, Bioresource Technology, 100, 2828–2831, 2009

VITA

Personal Information:

- Name: Emin Selahattin UMDU, Date of Birth: 29th May 1981, Nationality: Turkey
- E-Mail: selahattinumdu@gmail.com

Education:

- 2008-2012 PhD. in Chemical Engineering Department, Izmir Institute of Technology.
  Thesis: Hydrogen Production From Biomass Over Structured Catalysts
- 2006-2008 MSc. in Chemical Engineering Department, Izmir Institute of Technology.
  Thesis: Methyl Ester Production From Vegetable Oils On Heterogeneous Basic Catalysts
- 2000-2005 BSc. in Chemical Engineering Department, Izmir Institute of Technology.

Honors:

- Japanese Government (MONBUKAGAKUSHO:MEXT) Scholarshıp For 2012
- 2nd prize in the 1st Chemical Sector R & D Project Market, 28 December 2011
- 2nd rank in New Entrepreneurial Programme, June 2010
- Scholarship from The Scientific and Technological Research Council of Turkey (Tübitak) 01/02/2010 – 01/07/2010

Research Areas:

- Heterogeneous catalysis and its applications for renewable energy systems, namely hydrogen production and biodisel production over heterogeneous systems from biological feedstocks.
- Effect of building materials on energy efficiency and comfort in residential buildings.
- Polymer synthesis of acrylic ststems not containing residual monomers for dental applications.

Languages:

- Native Language: Turkish, Good Command of English (TOEFL IBT: 102), Beginner Japanese

Publications:

- Transesterification of sunflower oil on single step sol–gel made Al_2O_3 supported CaO catalysts: Effect of basic strength and basicity on turnover frequenc, Emin Selahattin Umdu, Erol Seker, Bioresource Technology November 11, 2011
- Transesterification of Nannochloropsis oculata microalga's lipid to biodiesel on Al2O3 supported CaO and MgO catalysts, Emin Selahattin Umdu, Mert Tuncer, Erol Seker, Bioresource Technology, 2009
- Biodiesel Production From Microalgae Over Heterogeneous Catalysts, M. Tuncer, E. S. Umdu, E. Kursat, G. Yilmaz, Y. Durmaz, S. Gokpinar, E. Seker, Global Conference On Global Warming Proceedings, İstanbul July 2008
- Biodiesel production from Canola oil over basic heterogeneous catalysts, Emin Selahattin Umdu, Erol Şeker, 2nd National Catalyst Congress Proceedings, Erzurum July 2008
- Biodiesel production with heterogeneous catalysts, Emin Selahattin Umdu, Erol Şeker, Biofuels and Biofuel Technologies Symposium Proceedings, Ankara December 2007
- Partial Purification of Hen Egg White Lysozyme by Ethanol Precipitation Method and Determination of the Thermal Stability of Its Lyophilized Form, Seyhun GEMİLİ, Emin Selahattin UMDU, Nilgün YAPRAK, Fatma Işk ÜSTOK, Fatih Yalçın Güneş YENER, Çiğem MECİTOĞLU GÜÇBİLMEZ, Sacide ALSOY ALTINKAYA, Ahmet YEMENİCİOĞLU, Turk Journal of Agriculture, 31, 2007

Important Activities:

- Project Executive in North Star and Firefly Project of ÇYDD İzmir Branch, 2010 → 2011
- Member of Educational Committee of Chamber of Chemical Engineers Aegean Branch, Turkey, 2010 →2011
- Participant in North Star and Firefly Project of ÇYDD İzmir Branch, 2009 → 2010
- Member of Energy Committee of Chamber of Chemical Engineers, Turkey, 2008 → 2010
- Member of LPG Committee of Chamber of Chemical Engineers, Turkey, 2008 → 2010
- Member of Executive Committee of Hydrogen Car Group, Car Chassis and Fuel Cell Teams, Izmir, Turkey, 2007 → 2009
- Member of Organizing Committee Assistants in "AzC IFToMM International Symposium on Mechanism and Machine Science 2010"
- Representative of İzmir Institute of Technology: Turkish University Students Assembly, Ankara, Turkey, December 2004.